Science of the Total Environment 871 (2023) 162064

Contents lists available at ScienceDirect

Science of the Total Environment

journal homepage: www.elsevier.com/locate/scitotenv

Climate variability of the southern Amazon inferred by a multi-proxy tree-ring approach using *Cedrela fissilis* Vell.

Daigard Ricardo Ortega Rodriguez [a,b,*], Raúl Sánchez-Salguero [b], Andrea Hevia [b,c], Daniela Granato-Souza [d], Bruno B.L. Cintra [e,f], Bruna Hornink [g,a], Laia Andreu-Hayles [h,i,j], Gabriel Assis-Pereira [a], Fidel A. Roig [k,l], Mario Tomazello-Filho [a]

[a] Universidade de São Paulo, Escola Superior de Agricultura Luiz de Queiroz, Departamento de Ciências Florestais, Av. Pádua Dias 11, 13418-900 Piracicaba, São Paulo, Brazil
[b] DendrOlavide-Dept. Sistemas Físicos, Químicos y Naturales, Universidad Pablo de Olavide, Crta. Utrera km. 1, 41013 Sevilla, Spain
[c] Department of Ecology, Universidad de Jaén, Campus Las Lagunillas s/n., 23009 Jaén, Spain
[d] Department of Geosciences, University of Arkansas, Fayetteville, AR 72701, USA
[e] Institute of Biosciences, University of São Paulo, Rua do Matão 14, São Paulo 05508-090, Brazil
[f] School of Geography, Earth and Environmental Sciences, University of Birmingham, Garstang North, Building, Birmingham B15 2TT, UK
[g] Department of Plant Biology, Institute of Biology, University of Campinas – UNICAMP, Campinas, São Paulo 13083-970, Brazil
[h] Lamont-Doherty Earth Observatory of Columbia University, Palisades, NY, USA
[i] CREAF, Bellatera (Cerdanyola del Vallès), Spain
[j] ICREA, Barcelona, Spain
[k] Argentine Institute of Nivology, Glaciology and Environmental Sciences (IANIGLA, CONICET-Universidad Nacional de Cuyo), 5500 Mendoza, Argentina
[l] Hémera Centro de Observación de la Tierra, Escuela de Ingeniería Forestal, Facultad de Ciencias, Universidad Mayor, Santiago, Chile

HIGHLIGHTS

- Long-term radial growth, density, inorganic chemistry and stable isotope series were developed.
- Chronologies extend back to 1835 CE local and regional climate variability.
- Tree-ring width, density and Ca and S concentration records mainly express local climate variability.
- The $\delta^{18}O$ record mostly reflects Amazon precipitation and sea surface temperature anomalies.

GRAPHICAL ABSTRACT

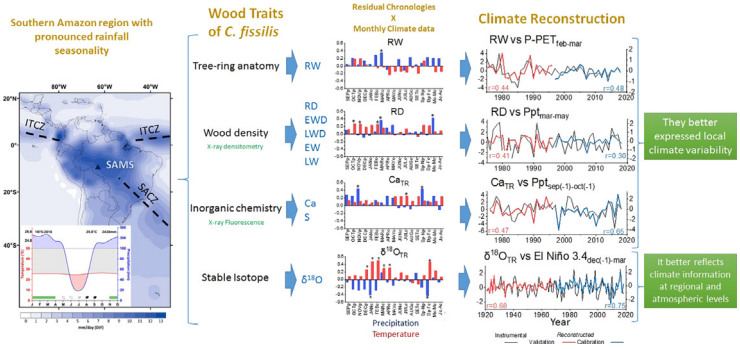

ARTICLE INFO

Editor: Manuel Esteban Lucas-Borja

Keywords:
Wood traits
Dendroclimatology
Dendrochemistry
Tropical forests
ENSO
SST

ABSTRACT

The analysis of climate variability and development of reconstructions based on tree-ring records in tropical forests have been increasing in recent decades. In the Amazon region, ring width and stable isotope long-term chronologies have been used for climatic studies, however little is known about the potential of wood traits such as density and chemical concentrations. In this study, we used well-dated rings of *Cedrela fissilis* Vell. from the drought-prone southern Amazon basin to assess the potential of using inter-annual variations of annually-resolved ring width, wood density, stable oxygen isotope ($\delta^{18}O_{TR}$) measured in tree-ring cellulose and concentration of Sulfur (S_{TR}) and Calcium (Ca_{TR}) in xylem cells to study climate variability. During wet years, *Cedrela fissilis* produced wider and denser rings with higher Ca_{TR} and lower S_{TR}, as well as depleted $\delta^{18}O_{TR}$ values. During dry years, a wider range of responses was observed in growth, density and S_{TR}, while lower Ca_{TR} and enriched $\delta^{18}O_{TR}$ values were found. The annual centennial

* Corresponding author at: Universidade de São Paulo, Escola Superior de Agricultura Luiz de Queiroz, Departamento de Ciências Florestais, Av. Pádua Dias 11, 13418-900, Piracicaba, São Paulo, Brazil.
E-mail addresses: dai.ricardo.or@gmail.com dai.ricardo.or@usp.br (D.R. Ortega Rodriguez).

http://dx.doi.org/10.1016/j.scitotenv.2023.162064
Received 4 October 2022; Received in revised form 11 January 2023; Accepted 2 February 2023
Available online 8 February 2023

chronologies spanning from 1835 to 2018 showed good calibration skills for reconstructing local precipitation, evapotranspiration (P-PET), Amazon-wide rainfall, as well as climate modes related to sea surface temperature (SST) anomalies such as El Niño South Oscillation (ENSO), Tropical Northern Atlantic (TNA), and the Western Hemisphere Warm Pool (WHWP) oscillations. Ca_{TR} explained 42 % of the variance of local precipitation (1975–2018), RW explained 30 % of the P-PET variance (1975–2018), while $\delta^{18}O_{TR}$ explained 60 % and 57 % of the variance of Amazon rainfall (1960–2018) and El Niño 3.4 (1920–2018), respectively. Our results show that a multi-proxy tropical tree-ring approach can be used for high-reliable reconstructions of climate variability over Amazon basin at inter-annual and multidecadal time scales.

1. Introduction

There is an increasing evidence of the importance of the Amazon forests for the hydrological cycle of the Amazon Basin and the atmospheric dynamics of South America (IPCC, 2021; Marengo et al., 2011; Marengo and Souza, 2018; Nobre et al., 2016). The Amazon Basin contributes almost 17 % of the global fresh water discharge to the Atlantic Ocean (Callède et al., 2010). The hydrological cycle in the Amazon Basin is tightly linked with the carbon cycle of the Amazon forest (Foley et al., 2002), which is one of the largest terrestrial biomass carbon pools (Malhi et al., 2006). Rainfall regimes across the Amazon basin have large spatiotemporal variations, which are influenced by modes of the Pacific and the Atlantic Ocean (e.g. El Niño-Southern Oscillation, Pacific Interdecadal Oscillation, Atlantic Multidecadal Oscillation, among others) on interannual, subdecadal and multidecal time scales (Espinoza et al., 2019; Jimenez et al., 2021; Marengo and Souza, 2018; Stahle et al., 2020). In most regions of the Amazon basin the South America Monsoon System (SAMS) and the Intertropical Convergence Zone (ITCZ) are the main drivers of seasonal precipitation regimes (Ancapichún et al., 2021; Marengo et al., 2012), which are also influenced by the above-mentioned modes. In addition, increasing anthropogenic disturbances, such as deforestation and associated fires, are also influencing hydroclimate variability in this region (Lovejoy and Nobre, 2018).

The southern region of the Amazon basin is very impacted by the variations of the SAMS and accordingly it exhibits an accentuated climate seasonality and variable lengths of the dry season (Agudelo et al., 2019; Cintra et al., 2021; Collini et al., 2008). Therefore, southern Amazon rainfall seasonality is controlled by Sea Surface Temperatures (SST) variations of the Eastern Pacific Ocean and the Tropical North Atlantic (Barichivich et al., 2018; Liebmann and Marengo, 2001; Lovejoy and Nobre, 2018; Marengo et al., 2008). In addition, increases in the length and severity of dry season have been recorded since approximately 1990 up to -20 mm month^{-1} (Gloor et al., 2015; Gloor et al., 2013).

Trends and changes in magnitude of the climatic processes have been evaluated at different resolutions in the Amazon basin by means of indirect paleoarchives such as tree rings (e.g. Cintra et al., 2021; Dünisch, 2005; Granato-Souza et al., 2020; Granato-Souza et al., 2018; Humanes-Fuente et al., 2020; Pucha-Cofrep et al., 2015; Schongart et al., 2004), lake sediments (e.g. Moreira et al., 2020) or speleothems (e.g. Novello et al., 2018; Vuille et al., 2012; Wang et al., 2017). In addition, tree rings and speleothems also served to evaluate climate variability in the southern Amazon region where the dry season is pronounced (e.g. Baker et al., 2016; Brienen et al., 2012; Brienen and Zuidema, 2005; Della Libera et al., 2022; Jenkins, 2009; Lopez et al., 2017).

Several wood traits of tree rings of Amazon species have been used to analyze and reconstruct climate variability (Boninsegna et al., 2009; Brienen et al., 2016). Tree-ring width chronologies provided centennial reconstructions of seasonal and annual precipitation in the equatorial Amazon (Granato-Souza et al., 2020; Granato-Souza et al., 2018), the Tropical Andes in regions that tribute to the Amazon River (Humanes-Fuente et al., 2020) and seasonally dry forests in the southern Amazon (Lopez et al., 2017). Isotope tree-ring chronologies (mainly based on $\delta^{18}O$) also proved to be excellent proxies for Amazon precipitation variability (Baker et al., 2016; Brienen et al., 2012; Cintra et al., 2019, 2021; Jenkins, 2009; Rodriguez-Caton et al., 2021; Volland et al., 2016). Significant correlations with Pacific SST anomalies were also reported in both ring width (Crispín-DelaCruz et al., 2022) and isotope (Rodriguez-Caton et al., 2022) chronologies. In addition, analysis of multidecadal frequencies based on a tree-ring width network correlated with the dry and wet periods observed across the Amazon basin (Humanes-Fuente et al., 2020; Pucha-Cofrep et al., 2015).

Other physical and chemical parameters have been less used for dendroclimatic analysis in tropical regions. While tree-ring width and density reflect ontogenetic and enviromental changes in tree growth, chemical concentrations in tree-ring wood may reflect physical conditions of the soil and tree responses to soil nutrients availability (Balouet et al., 2009; Hevia et al., 2018; Ortega Rodriguez et al., 2022; Sánchez-Salguero et al., 2019). Therefore, physical and chemical wood properties can provide complementary climatic information in areas where the relationships between climatic variables (monthly or seasonal) and ring width are complex, unstable or weak (Poussart et al., 2006; Sánchez-Salguero et al., 2019).

Wood density is based on the wood volume allocation among the different xylem tissues (Janssen et al., 2019), and similar to ring width is driven by environmental conditions, such as temperatures and water availability (Björklund et al., 2019; Briffa et al., 2002; Schweingruber et al., 1978). Worbes et al. (1995) built chronologies of maximum wood density of *Macrolobium acaciifolium* (Benth.) Benth. and *Swartzia polyphylla* DC. that showed a positive association with the duration of the non-flood phase in the Central Amazon floodplains. In a similar floodplain area, Gonçalves et al. (2021) obtained positive correlations between mean wood density of the whole ring (RD), earlywood (EWD) and latewood (LWD) of *Nectandra amazonum* Nees and minimum temperature and evapotranspiration, and a weak correlation of RD and EWD with the SST of the TNA, mainly during the lower-water period and the transition between the dry and the wet seasons.

Regarding the chemical concentrations in wood, their transport and storage in the xylem depend on the trees' capacity to uptake nutrients by roots (primarily via) from the soil solution (Cutter and Guyette, 1993). The soil is intricately linked to the atmospheric system; hence any change in climate is expected to influence soil characteristics (Yuan et al., 2017) and soil exchangeable cation pool available for trees (Hevia et al., 2018). Furthermore, some elements can be detected in the wood formed before or after the period of absorption of the element, due to the characteristics of mobility and transport path of the element or the functionality of the sapwood (Smith and Shortle, 1996). Calcium (Ca), an immobile element, acts as an important regulator in processes such as stomatal conductance rates, cell division and cell-wall synthesis (Fromm, 2010; Lautner and Fromm, 2010). Poussart et al. (2006) found significant positive correlations between the rainfall corresponding to the end of the dry season of the northern Thailand monsoon and the annual maximum intensities of Ca in *Miliusa velutina* (A.DC.) Hook.f. & Thompson. Sulfur (S), a mobile element, can be used directly for protein synthesis and, therefore, for the growth and development of different tree parts (Fairchild et al., 2009). Herschbach and Rennenberg (2001), working with deciduous trees from the temperate climate zones, verified that S accumulation in storage tissues of the xylem occurs during spring and xylem unloading seems to take place in late summer and autumn.

As a novelty approach, we use tree-ring time series of different wood traits to study climate variability on various spatial and temporal scales. Our main objective is to assess the potential of annual tree-ring width, wood density, $\delta^{18}O$ and relative concentration of Ca and S in wood of

Cedrela fissilis Vell. to serve as proxies of climate variability in a moist tropical forest with pronounced rainfall seasonality in southern Amazon. We (1) assess the strength of the local, regional and global large-scale climate drivers of the Amazon basin in these tree-ring parameters and (2) evaluate the potential of a multi-proxy tree-ring approach for developing long-term dendroclimatic reconstructions in the Amazon Basin.

2. Material and methods

2.1. Study area

The study site is located in the Jamari National Forest (JNF), in an area under permanent forest management conducted by the logging company AMATA. JNF is located in the southern Amazon basin, at the north limit of the state of Rondônia, Brazil (09°00′ to 09°30′ S and 62°44′ to 63°17′ W; altitude 115 m.a.s.l.; MMA - Ministério Do Meio Ambiente, 2005) (Fig. 1). The region exhibits a strong seasonal variability mostly driven by the SAMS (Marengo et al., 2012; Novello et al., 2017) (Fig. 1a). The average annual rainfall (P) in this region is 2438 mm, and the annual average temperature is 26 °C (Fig. 1b). The site is classified as a moist forest exposed to seasonality in water availability (Guan et al., 2015), with a dry season from June to August and potential evapotranspiration (PET) exceeding precipitation from June to September. Fig. 1c shows how since 1975 this region experienced a significant negative trend in annual precipitation ($r = -0.28$, $p < 0.05$; Mann-Kendall Z_{MK} value $= -0.57$, $p = 0.57$), a significant negative significant trend in P-PET ($r = -0.39$, $Z_{MK} = -2.47$, $p < 0.05$) and a positive trend in annual temperatures ($r = -0.85$, $Z_{MK} = 6.3$, $p < 0.05$) (Table S1) (Ritchie et al., 2022).

2.2. Fieldwork and sample preparation

Wood discs were cut at the top level of the first log (6 m) (Granato-Souza et al., 2018) from 29 living and dominant trees of *Cedrela fissilis*, which were felled and stored in log yards between April and May of 2019. Three to four radial samples (10 cm width and 5 cm thickness) from each disc were cut and transported to the Wood Anatomy and Tree-Ring Laboratory, ESALQ, University of Sao Paulo (LAIM/ESALQ/USP) to be air dried (Fig. 2a). The radial samples were polished gradually with sandpaper (from 80 to 600 grains $inch-2$) until tree rings were clearly visible. The radii were cross-dated using both skeleton plots and visual dating under the microscope (Stokes and Smiley, 1996). Each cross-section was scanned at 1200 dpi resolution with Epson Expression 10000XL scanner and the width of the annual rings (RW) of the synchronized samples were measured with a resolution of 0.01 mm using CDendro and CooRecorder ® software (Cybis Electronic, 2013) (Fig. 2b). The Schulman convention (Schulman, 1956) was not applied to the calendar dating of the JNF series, which means that for instance, the tree ring formed from austral spring 2017 to austral fall 2018, was assigned to the year 2018. For each radial sample three thin radial-section (2 cm width and 1.7 to 4 mm thickness) were cut transversely for wood density, inorganic chemical and stable isotope analysis.

Wooden laths from 29 trees were extracted for densitometric analyses and were kept under constant temperature and humidity (20 °C and 60 %, respectively) for 48 h in a 12 % moisture content atmosphere (Quintilhan et al., 2021; Tomazello-Filho et al., 2008). The samples were then scanned with a calibration scale of cellulose acetate using an X-ray densitometry chamber (Faxitron MX20-DC12, Faxitron X-Ray, Illinois, USA). The digital X-Ray images of cross-section samples were analyzed with WinDendro Density 2017a® software (Regent Instruments Inc., Canada), obtaining a density profile with 15 μm intervals. The position of the earlywood-latewood boundary was defined following Ortega Rodriguez et al. (2022) (Fig. S1). Then, the specific wood density time series of each radii for the whole ring (RD), earlywood (EWD) and latewood (LWD) expressed in $g\ cm^{-3}$ were produced using WinDendro software (Fig. 2c).

Wooden laths were extracted from 14 trees for chemical analyses and were kept under controlled conditions (20 °C temperature and 50 % humidity) before micro X-ray Fluorescence (μXRF) analysis in an ItraxMultiscanner (Cox Analytical Systems, Sweden) at the laboratory of DendrOlavide, Universidad Pablo de Olavide (Seville, Spain). Itrax was operated at 30 KV and 50 mA with a Cu-tube, and samples were exposed to the X-ray beam for 40 s at each measurement point in radial direction (20-μm step size). Count rates of fluorescent photons of elements and a radiographic greyscale image in each measurement point of each sample were obtained. Peaks in the μXRF spectrum were assigned to specific elements using the Q-spec software (Cox Analytical Systems, Sweden), producing relative concentrations (counts of fluorescent photons per second, cps) (e.g., Croudace et al., 2006) of those elements detected within the wood structure for every analyzed point. The radiographic images were cross-dated with previously built chronologies in each site to assign the element specific count rates to each annual ring using WinDendro™ (Regent Instruments Inc., Canada). Mean annual time series for each radii were produced considering the following detected elements with higher concentration in the wood cells: Calcium (Ca) and Sulfur (S) (Fig. 2d).

Wooden laths from a total of six trees were selected for isotopic analyses and were cut using a core-microtome WSL (Birmensdorf, Switzerland) (Gärtner and Schweingruber, 2013). Cellulose extraction was performed following the protocol described in Wieloch et al. (2011), adapted for the LES/IGc/USP. Samples were immersed twice in an alkaline solution of 5 % NaOH for 2 h (total 4 h), then washed three times with boiling water and immersed four times in acidified solution of 7.5 % $NaClO_2$ with pH between 4 and 5, adjusted with acetic acid. Samples were then washed three times with boiling water, placed on histological slides, dried in an oven chamber at 40 °C for up to 2 h, frozen at least 48 h and finally freeze-dried to completely remove moisture from the material. The tree rings were separated from the extracted cellulose lath using a BIC's chrome platinum blades (Clichy, France) and homogenized. The homogenized cellulose of each ring was then weighed in a high precision microbalance and packed in silver capsules. The $\delta^{18}O$ measurements were performed with a Thermo Element Analyzer (Flash EA Isolink) coupled to a CONFLO IV and Delta V Isotope Ratio Mass Spectrometer, at the LES/IGc /USP (Fig. 2e).

2.3. The multi-proxy tree-ring chronologies

The cross-dating among the tree-ring width and density series was evaluated using the COFECHA program (Holmes, 1983) using 30-year intervals lagged 15 years. The annual periodicity of the same samples used in this study was previously confirmed using the radiocarbon "bomb-peak" dating (Santos et al., 2021). Fourteen radii from 14 trees, which presented the best correlations statistics with the mean site series of width and density, were selected to generated the chemical (S, Ca) chronologies. To obtain comparable ring-width, −density and -chemical series of each tree and remove the age- size-related trend and non-climatic signals cross-dated raw series were standardized and detrended using the ARSTAN program (Cook and Krusic, 2005). Only for the chemical series, a horizontal line function through the mean (which did not change the shape of the series) was initially applied as an alternative for normalizing the raw data. The individual raw ring-width, density and chemical series were detrended by fitting a 30-year spline to retain high-frequency variability to obtain standardized ring indices. These individual standardized series were averaged to obtained the standard chronologies for ring-width (RW), earlywood width (EW), latewood width (LW), ring density (RD), earlywood density (EWD), latewood density (LWD), and relative concentration of Sulfur (S_{TR}) and Calcium (Ca_{TR}) in the ring. In addition, the autocorrelation was removed from the individual standardized series using an autoregressive model (Cook, 1985) to obtain the individual residual series that were averaged using a robust mean to generate the residual chronologies. A variance stabilization technique was applied to every single series for minimizing the effects of changing sample size throughout time (Frank et al., 2007), improving the final chronology statistics. Finally, the individual $\delta^{18}O$ series from six *Cedrela fissilis* trees were averaged to develop the oxygen isotope chronology ($\delta^{18}O_{TR}$), which was not detrended.

All the wood trait chronologies were evaluated using dendrochronological statistics including the mean correlation among all time series (rbar;

Cook and Pederson, 2011), the first-order autocorrelation (AC), the mean sensitivity (MS), and the Expressed Population Signal (EPS; Wigley et al., 1984) (Table 1). Climate analyses were performed for the periods when the chronologies show the statistic EPS equal or higher than 0.85, with the exception of the chemical chronologies (S_{TR} and Ca_{TR}) that were used with high EPS values albeit not reaching 0.85 (Table 1). Morlet-Wavelet

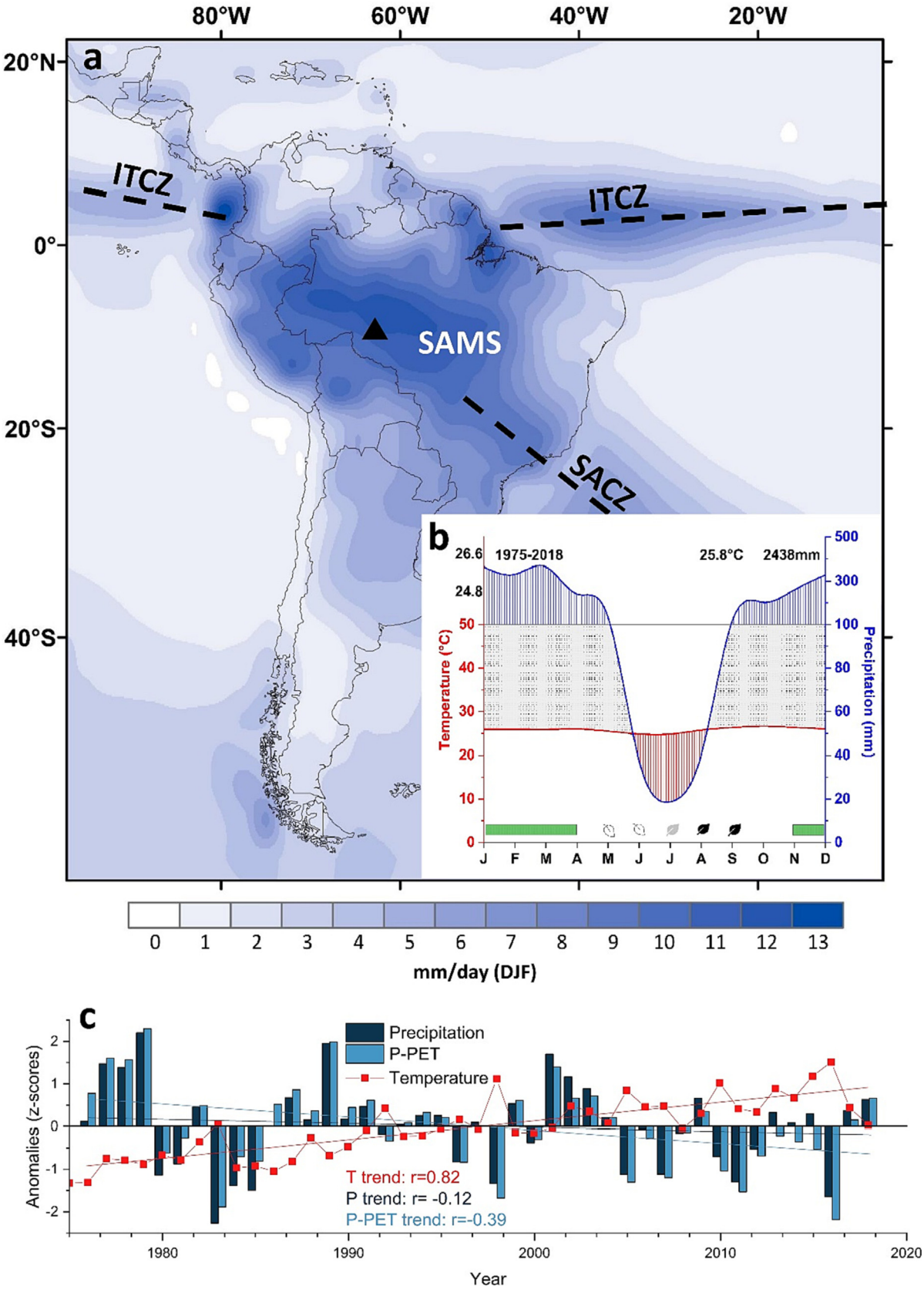

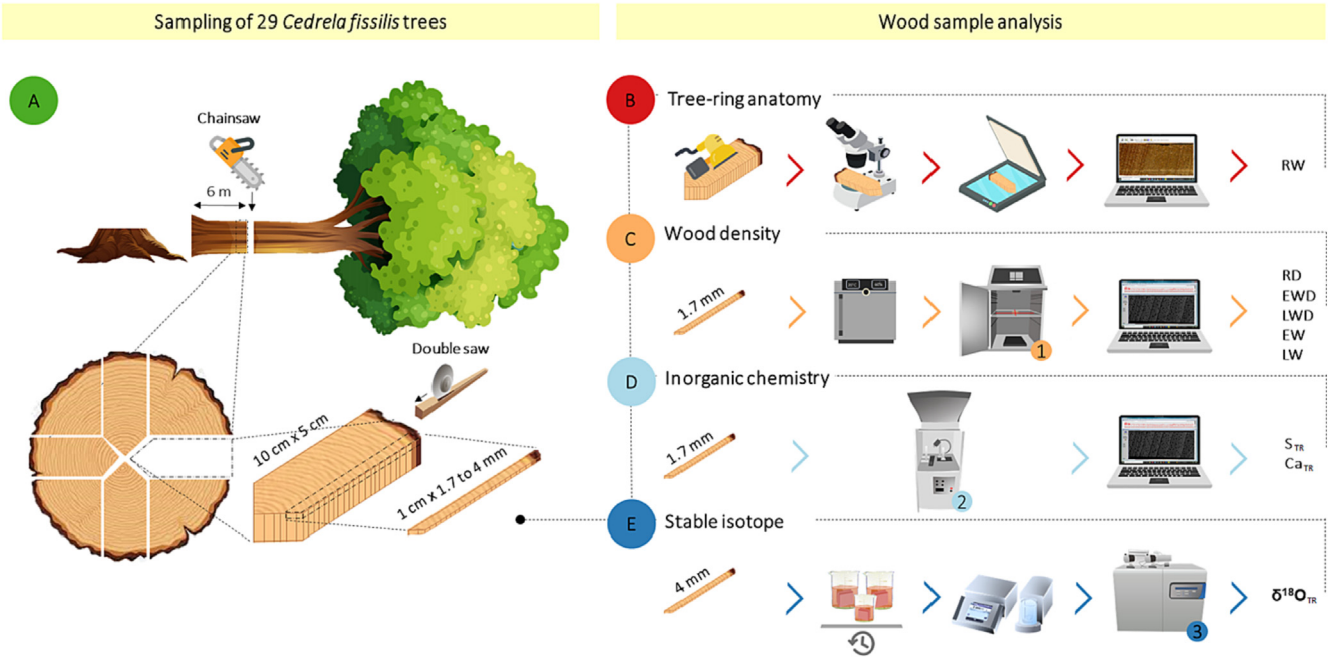

Fig. 2. a) Schematic figure of disc collection and preparation of subsamples for: b) macroscopic wood anatomy analysis for ring width (RW) measurement (29 trees); c) X-ray microscopy analysis of wood density profiles to obtain ring (RD), earlywood (EWD) and latewood (LWD) density, and earlywood (EW) and latewood (LW) width (29 trees); d) X-ray fluorescence microscopy analysis of chemical profiles to obtain ring Sulfur (S_{TR}) and Calcium (Ca_{TR}) relative concentrations (14 trees; and e) stable isotope analysis to obtain $\delta^{18}O_{TR}$ (6 trees). Equipment used: 1) X-ray densitometry chamber (Faxitron MX20-DC12, Faxitron X-Ray, Illinois, USA); 2) micro X-ray Fluorescence (μXRF) ItraxMultiscanner (Cox Analytical Systems, Sweden); and 3) Delta Thermo Scientific magnetic sector mass spectrometer.

analysis (MW, Torrence and Compo, 1998) were also applied to study changes in the frequency domains over the total length of the wood traits residual chronologies. The chronology building and the MW analysis were performed using the "dplR" package in the R environment (R Core Team, 2019).

2.4. Climate, hydrological and oceanic data

To obtain long and reliable series of monthly climate data we created regional mean precipitation and temperature series from five and six local meteorological stations, respectively (Table S1). We used the HOM and MET programs from DPL version 1.05 (Krusic, 2006) to estimate missing data and calculate the regional time series. To evaluate large-scale hydrological variation, we obtained monthly Amazon-wide rainfall series from Climate Reaseach Unit (CRU TS 4.04) for the region 8°-10°S and 62°-64°W. As a metric that express drought intensity, we used the difference between precipitation (P) and evapotranspiration (PET) (Vicente-Serrano et al., 2010). The PET was calculated using the *SPEI* package (Vicente-Serrano et al., 2010) in R environment (R Core Team, 2021). To examine the teleconnections and influence of large-scale oceanic modes we obtained from the NOAA website (National Oceanic and Atmospheric Administration; https://psl.noaa.gov/data/climateindices/list/) monthly sea surface temperature (SST) anomalies of Tropical Northern (TNA) and Southern Atlantic (TSA), Atlantic Multidecadal Oscillation (AMO), Western Hemisphere Warm Pool (WHWP) and El Niño/Southern Oscillation (El Niño 3.4).

2.5. Climate-wood traits analysis

To quantify associations between wood traits and monthly climate data, we calculated bootstrapped Pearson correlation coefficients for the common periods 1975–2018 for local precipitation, temperature and P-PET; 1959–2018 for Amazon-wide rainfall; 1920–2018 for El Niño 3.4 and AMO; and 1950–2018 for TNA, TSA and WHWP. These correlations were calculated monthly from September of the previous year to September of the current year, which include the period of the tree-ring formation from prior September to current May (Lobão, 2011). We also calculated seasonal correlations considering the beginning of the rainy season (prior September to November), middle of rainy season (prior December to current February), end of the rainy season (current March to May) and dry season (current June to August). Spatial correlations were computed between gridded precipitation from the Climate Research Unit (CRU TS 4.00 0.5° resolution (Harris et al., 2020) and (1) the regional precipitation series computed for this study (Table S1) to test the quality of the database in the region. (Vicente-Serrano et al., 2010), and (2) the newly developed wood traits chronologies to test their potential as climate proxies. We also analyze the stability of the climate signal in wood trait chronologies over time. The variability of the wood traits was ordinated through a principal

Fig. 1. a) Map showing the location of Jamari National Forest, JNF (black triangle). It also highlights the South American Monsoon System (SAMS) and shows the position of the Intertropical and South Atlantic convergence zones (ITCZ and SACZ) during the austral summer in South America (December to February, DJF) based on the dataset of Novello et al. (2017). b) The Climate diagram of Walter & Lieth, based on regional meteorological and hydrological records from 1975 to 2018 (data source in Table S1), indicates dry months (solid orange area) and the months with rainfall above 100 mm (solid blue areas). Green bars represent the estimated growing period of *Cedrela fissilis*, which generally falls between September (previous year) and the end of May (current year) according to Lobão (2011). Phenology stages are represented by leaf icons based on *C. fissilis* data from Lobão (2011): open, gray filled and dark filled indicate periods of leaf-fall, leaf-flash and leaf-fall /leaf-flash (occurring simultaneously), respectively. c) Bar plots show anomalies (standardized values) of total annual precipitation (P), total annual difference between precipitation and potential evapotranspiration (P-PET), and mean annual temperature (T). Climate data were obtained from the Agência Nacional de Águas (ANA, National Water Agency) and the Instituto Nacional de Pesquisas Espaciais (INPE, National Institute of Space Research) (see Table S1).

Table 1
Tree population features and statistical characteristics of tree-rings series.

Location	DBH (cm)	Tree height (m)		Age at 6 m (years)		Specific gravity (g cm^{-3})	
Jamari Nat. For.	73.7 ± 2.8	15.3 ± 0.5		83 ± 6		0.4 ± 0.07	
Dendrochronological Statistics	N° trees / N° radii	Value	rbar	AC	MS	Chronology length	Time span (EPS)
RW (mm)	20/62	2.33 ± 1.19	0.31	0.52	0.40	1840–2018	1895–2018 (0.93)
EW (mm)	15/45	1.19 ± 0.74	0.29	0.46	0.50	1842–2018	1895–2018 (0.91)
LW (mm)	12/32	1.04 ± 0.59	0.25	0.35	0.48	1896–2018	1930–2018 (0.89)
RD (g cm^{-3})	15/40	0.49 ± 0.05	0.29	0.56	0.07	1835–2018	1945–2018 (0.91)
EWD (g cm^{-3})	13/36	0.48 ± 0.06	0.24	0.38	0.11	1880–2018	1950–2018 (0.89)
LWD (g cm^{-3})	9/27	0.62 ± 0.06	0.23	0.46	0.08	1858–2018	1950–2018 (0.88)
$\delta^{18}O_{TR}$ (‰)	6/6	23.61 ± 1.36	0.64	−0.05	0.07	1909–2018	1909–2018 (0.91)
S_{TR} (cps)	7/7	31.59 ± 7.22	0.30	0.63	0.08	1868–2018	1955–2018 (0.76)
Ca_{TR} (cps)	4/5	6664.14 ± 1907.59	0.26	0.53	0.10	1897–2018	1975–2018 (0.66)

Abbreviations: Ring width (RW), earlywood width (EW), latewood width (LW), tree-ring density (RD), earlywood density (EWD), latewood density (LWD), stable oxygen isotope ($\delta 18O_{TR}$), relative tree-ring concentrations of Sulfur (S_{TR}) and Calcium (Ca_{TR}); DBH, diameter at breast height; mean correlation of index values among all series (rbar); first-order autocorrelation for raw tree-ring series (AC); mean sensitivity (MS); Expressed Population Signal (EPS).

component (PC) analysis and was calculated a 10-year long moving correlation lagged by one year between the first, second and third PC scores and the local precipitation and temperature, Amazonian precipitation and SSTs El Niño 3.4, TNA and WHWP.

2.6. Climatic reconstructions

Reconstructions models used as observations the tree-ring chronologies and as targets normalized series (*Z*-scores, i.e., the mean was subtracted from each value and divided by the standard deviation) of precipitation, P-PET totals, as well as El Niño 3.4, TNA and WHWP indices. Each variable had a reconstruction model that used half of the data for calibration and the other half for verification. The explained variance between observed and predicted values for each model was assessed by the correlation coefficient r (r_{adj}) with $p < 0.05$; the coefficient of determination adjusted for loss of degrees of freedom R^2 (R^2_{adj}); the reduction of error (RE) statistics (Cook et al., 1994; Fritts, 1976), which accounts for the relationship between actual value and estimates;. the root mean square error of validation ($RMSE_v$; Weisberg, 1987) that estimates the uncertainties of the reconstructions; and the Durbin-Watson (DW) test (Ostrom, 1990) that determines the degree of auto-correlation of the residuals. Analyses to assess the climate-growth relationships were calculated using the *treeclim* package (Zang and Biondi, 2015) in the R environment (R Core Team, 2021). Figures editing was carried out using the software OriginLab 2018 (OriginLab Corporation, 2018).

3. Results

3.1. Wood traits chronologies

Box plots suggest that *Cedrela fissilis* form rings wider (RW, EW, LW), denser (RD, EWD, LWD), with higher Ca_{TR} but lower S_{TR} concentrations and more depleted $\delta^{18}O_{TR}$ during wet years compared to narrower, less dense, with lower Ca_{TR} but higher S_{TR} concentrations and more enriched in $\delta^{18}O_{TR}$ in dry years (Fig. S2; Table S2).

All the standardized chronologies are presented in Fig. 3, while their descriptive statistics are shown in Table 1. The RW chronology was based on 62 radii from 20 *Cedrela fissilis* trees (69 % of all sampled trees) and had a significant mean correlation among the series ($r = 0.51$, $p < 0.01$; rbar = 0.31). The RW chronology spanned from 1840 to 2018, but it was statistically reliable from 1895 to 2018 (EPS > 0.85). The microdensity chronologies comprised a total 45 (EW), 32 (LW), 40 (RD), 36 (EWD) and 27 (LWD) radii from 15, 12, 15, 13 and 9 trees, which represent the 52 %, 41 %, 52 %, 45 % and 31 % of all sampled trees, respectively. The highest correlations among the trees were found for the reliable time span (EPS > 0.85) for EW (1895–2018, rbar = 0.29), LW (1930–2018, rbar = 0.25), RD (1945–2018, rbar = 0.29), EWD (1950–2018, rbar = 0.24) and LWD (1950–2018, rbar = 0.23). The tree-ring $\delta^{18}O_{TR}$ record (1909–2018, rbar = 0.64), as well as the chemical chronologies of S_{TR} (1868–2018, rbar = 0.30) and Ca_{TR} (1897–2018, rbar = 0.26) presented significant mean correlation coefficients among the series (see Table 1). The wavelet analysis showed significant periodicities across the wood traits chronologies (Fig. S3). Specifically, strong significant oscillatory modes associated with interannual to subdecadal variability (1–8 years) and decadal to multidecadal variability (10–40 years) were observed for almost all variables.

3.2. Local, regional and global climate sensitivity of wood traits

Spatial correlations between the CRU gridded precipitation dataset and the monthly instrumental precipitation observations from the southwestern Amazon collected in the present study (Table S1) were positively only during the dry season months from May to August (Figs. S4a, b and c). Furthermore, two wood trait chronologies presented weak correlations with the CRU gridded precipitation, $\delta^{18}O_{TR}$ negatively with January to February and S_{TR} positively for August to October, while the rest showed non-significant correlations (RW, RD and Ca_{TR}). Therefore, due to the weak correlations obtained with the CRU database for the region with both local instrumental data and proxies, further climate analyses were carried out with local instrumental data (Table S1).

Correlation between *Cedrela fissilis* wood trait chronologies and local instrumental precipitation showed that tree growth and density were enhanced during the rainy season (Fig. 4), particularly from February to March (RW, r = 0.44; EW, r = 0.44; LW, r = 0.37; EWD, r = 0.43), March to May (RD, r = 0.44) and March to April (LWD, r = 0.43) (Figs. 3 and 4). October–November temperatures during the rainy season positively correlated with EW and ring density (RD, EWD, and LWD). During the rainy season $\delta^{18}O_{TR}$ correlated positively with January to February temperature (r = 0.47), while S_{TR} concentrations correlated negatively with February to March temperatures (r = −041) (Fig. 4, S5a and b). Prior September–November precipitations and January precipitation during the growing season positively correlated with concentrations of Ca_{TR} (r = 0.47) (Figs. 3 and 4) and negatively correlated with $\delta^{18}O_{TR}$, respectively. August–October precipitations during the beginning of the next rainy season positively correlated with S_{TR} concentrations (r = 0.53) (Figs. 3 and 4).

Regarding the sensitivity of the tree-ring chronologies to Amazon-wide rainfall, rain during previous year October and current year December (months at the beginning of the rainy season) negatively correlated to tree growth (RW, EW and LW) and density (RD, EWD, LWD) (Fig. S6a and b). The $\delta^{18}O_{TR}$ was also negatively associated with Amazon rainy season precipitation but mainly during prior year November to current year March (r = −0.76) (Fig. 3 and S6c).

The correlations between P-PET and the wood traits showed that February low evapotranspiration positively affect tree growth (RW, EW

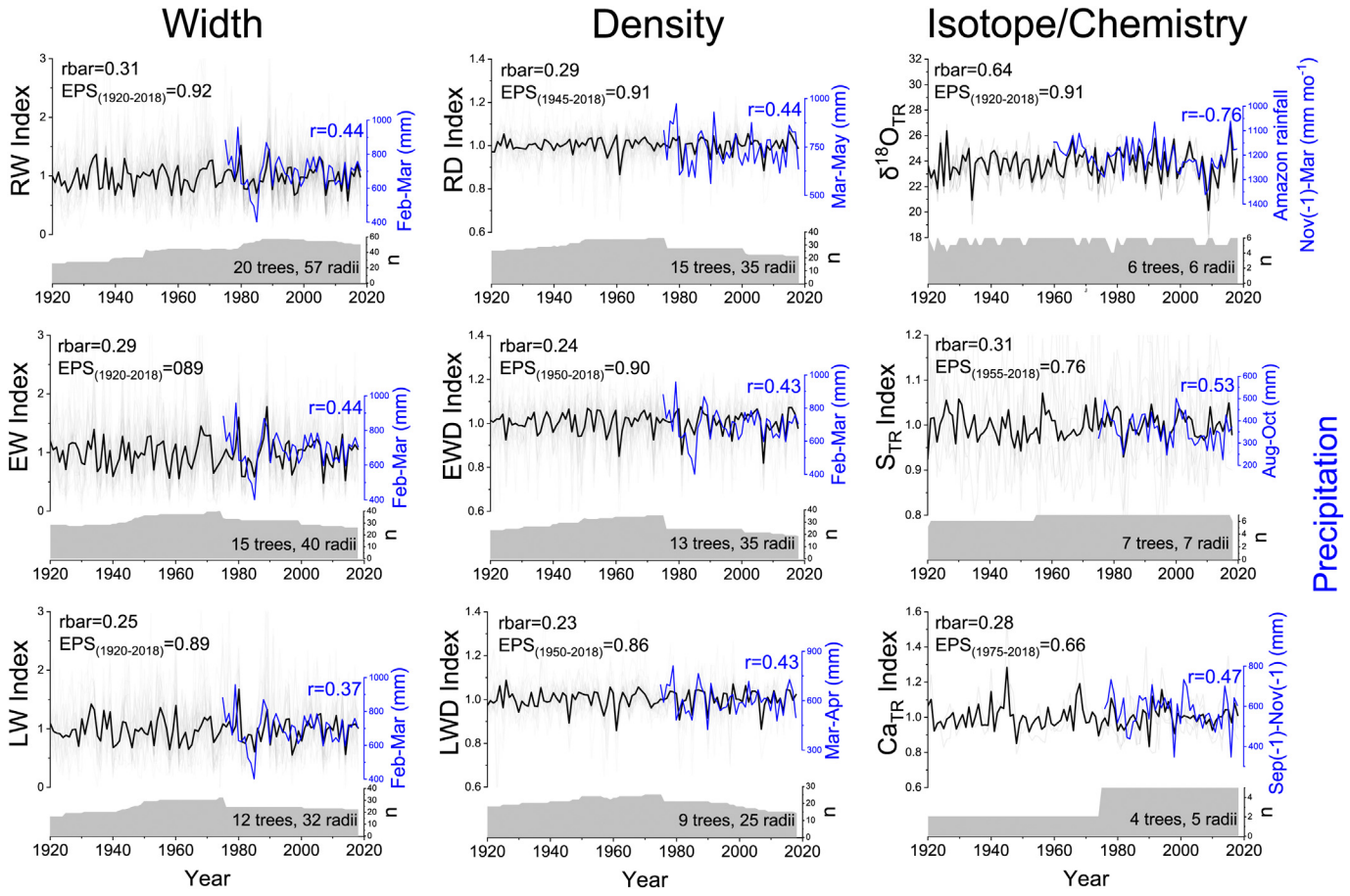

Fig. 3. Mean index residual chronologies (black lines), individuals (light gray lines) and number of trees and radii (bottom gray shading) of tree-ring width for the whole ring (RW), earlywood (EW), latewood (LW) and the associate wood density (RD, EWD and LWD, respectively), as well as the $\delta^{18}O_{TR}$ ratio and concentrations of Sulfur (S_{TR}) and Calcium (Ca_{TR}). All the wood traits chronologies are shown for the common period 1920–2018 with the mean correlations among all radii within each chronology (i.e., rbar between 0.23 and 0.64). The EPS of all the tree-ring chronologies was above the arbitrary 0.85 EPS threshold, except for the S_{TR} and Ca_{TR} tree-ring chronologies. The southern Amazon precipitation (Blue lines) is indicated for the months of maximum seasonal signal, based on monthly correlation analyses (Fig. 4). The Pearson correlation coefficient between precipitation each wood trait chronology ($p < 0.01$) is depicted in blue in each plot. For S_{TR}, we presented current year August to October precipitation since the reallocation and storage of this element in the prior formed ring may occur at the beginning of the next rainy season (Herschbach and Rennenberg, 2001).

and LW; Fig. S6d) and seasonally, the highest correlation were obtained from February to March P-PET (r = 0.44; Fig. S5d). The $\delta^{18}O_{TR}$ was negatively associated with January P-PET totals (Fig. S6f) and seasonally the highest correlation was obtained with prior October to February P-PET totals (r = −0.46; Fig. S5c).

Regarding large-scale global climate sensitivity, SST anomalies and wood traits associations were observed (Fig. S7), with the highest correlations shown by the $\delta^{18}O_{TR}$ record (Fig. 5). El Niño 3.4 presented negative correlations with tree-ring radial growth (RW, EW, LW) and positive correlations with $\delta^{18}O_{TR}$ during the local rainy season from January to May (Fig. S7a) and prior September to May (Fig. S7c), respectively. More specifically, seasonally El Niño 3.4 and $\delta^{18}O_{TR}$ association showed the highest positive correlation (r = 0.68) during previous December to current March (Fig. 5b). The WHWP anomalies showed positive correlations with $\delta^{18}O_{TR}$ and negative correlations with tree-ring growth (RW) during the local rainy season from prior December to May (Fig. S7f) and March to April (Fig. S7d), respectively. Seasonally, the WHWP and $\delta^{18}O_{TR}$ association was positive (r = 0.45) during previous December to current March (Fig. 5b). The AMO presented positive correlations with LW growth during the local dry season from July to August (Fig. S7g). The AMO and TNA presented positive correlations with $\delta^{18}O_{TR}$ during the end of the local rainy season and the beginning of the dry season from February to June (Fig. S7i and l). Seasonally, the highest significant correlation (r = 0.42) was obtained for TNA and $\delta^{18}O_{TR}$ from February to May (Fig. 5b). The TSA only exhibited significant correlations with RD in the dry season (July of the current year) (Fig. S7n).

3.3. Dendroclimatic reconstructions

The tree-ring wood traits chronologies showed reliable models with significant statistics for reconstructing local, regional and global climatic variables (Fig. 6 and Table 2). The highest correlations between instrumental and reconstructed local precipitation for prior September–October were obtained using the Ca_{TR} chronology with correlation values of 0.65 and 0.47 for calibration (1997–2018) and validation period (1975–1996), respectively (Fig. 6). The chronologies explained the following % of the variance for distinct seasonal instrumental precipitation: February–March (34 % EW), March–May (10 % RD), August–October (31 % S_{TR}) and prior September-prior October (42 % Ca_{TR}) during the calibration period, whereas for the validation period the R^2_{adj} was 0.20, 0.26, 0.18 and 0.17, respectively. According to the Durbin-Watson test, the residuals of the almost all regression models were not significantly autocorrelated (DW = 2), which means that the effect of past climate on tree growth and physiology that is propagated forward in time was removed (Fritts, 1976). Almost all models (except the Ca_{TR} model) successfully passed the verification process (positive RE and significant $RMSE_v$), which implies significant predictive accuracy of the tree-ring chronologies to infer past changes in local precipitation of the southwestern Amazon.

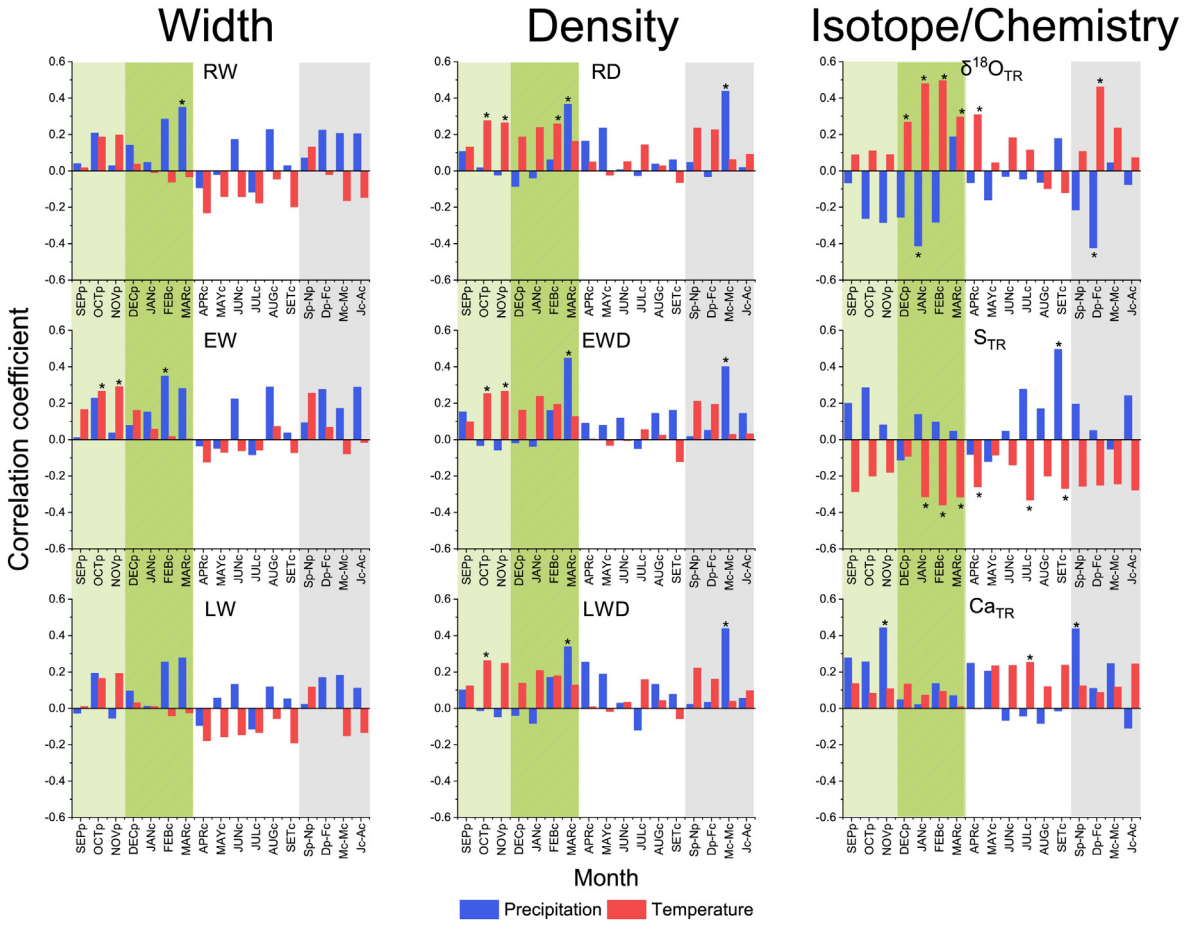

Fig. 4. Pearson correlation coefficients between tree-ring width (RW, EW, LW), density (RD, EWD, LWD), isotopic ($\delta^{18}O_{TR}$) and chemical (S and Ca) residual chronologies with monthly precipitation and temperature from 1957 to 2018. The light green shading includes the rainy months for the study region and the dark green vertical box with line pattern shows the *Cedrela fissilis* growing period based on Lobão (2011). Gray shading shows the seasonal correlations. Asterisks above and below the bars show the significant level ($p < 0.05$). For S_{TR}, we extended the monthly correlation to September of the current year because its reallocation and storage in the prior formed ring may occur at the beginning of the next rainy season (Herschbach and Rennenberg, 2001).

At a regional-scale, the $\delta^{18}O_{TR}$ chronology explained 60 % of prior November–March Amazon-wide rainfall during the calibration period (1989–2018) and had a 0.29 R^2_{adj} for the validation period (1960–1988) (Fig. 6). The instrumental and reconstructed Amazon-wide rainfall correlations were 0.77 for calibration (1989–2018) and 0.70 for validation (1960–1988) period. DW test showed a slightly positive autocorrelation in the regression model (DW < 2), but acceptable predictive accuracy (positive RE and significant $RMSE_v$) for the $\delta^{18}O_{TR}$ chronology to reconstruct Amazon precipitation. The RW and $\delta^{18}O_{TR}$ chronologies showed also potential for reconstructing drought intensity (P-PET). The RW and $\delta^{18}O_{TR}$ chronologies explained 30 % and 20 % of February–March and prior October–February P-PET during the calibration period (1997–2018), respectively. Instrumental and reconstructed P-PET correlation was 0.48 and 0.44 (based on the RW model) and 0.44 and 0.45 (based on the $\delta^{18}O_{TR}$ model) for calibration (1997–2018) and validation (1975–1996) periods, respectively. Non-significant autocorrelation was found in the residuals (DW = 2). Positive RE and significant $RMSE_v$ were also obtained.

Regarding large-scale reconstructions, the $\delta^{18}O_{TR}$ record explained 57 %, 10 % and 30 % during the calibration period for El Niño 3.4 (prior December–March;1969–2018), TNA (February–May; 1984–2018) and WHWP (prior December–March; 1984 to 2018) SSTs global anomalies. For the validation period the following R^2_{adj} were obtained for El Niño 3.4 (R^2_{adj} = 0.32; 1921–1968), TNA (R^2_{adj} = 0.18; 1950 to 1983), and WHWP (R^2_{adj} = 0.17; 1950 to 1983). Finally, instrumental and reconstructed El Niño 3.4, TNA and WHWP correlation was 0.75, 0. 31 and 0.65 for calibration and 0.68, 0.35 and 0.50 for validation period, respectively. Non-significant autocorrelation was found in the residuals (DW = 2). Positive RE and significant $RMSE_v$ were also obtained for the regression models to reconstruct SSTs global anomalies using the $\delta^{18}O_{TR}$ record.

3.4. Climate signal stability in wood traits

Fig. S8 showed the temporally correlation analysis between climate and wood trait principal components. The wood traits were ordered by a principal component analysis: PC1, which explains 46 % of the variance and discriminates significant correlations with a positive loading of RW (r = 0.41), EW (r = 0.43), LW (r = 0.37), RD (r = 0.41), EWD (r = 0.42) and LWD (r = 0.39); PC2, which explains 16% of the variance and discriminates significant correlations with a positive loading of $\delta^{18}O_{TR}$ (r = 0.65); and PC3, which explains 12% of the variance and discriminates significant correlations with a positive loading of S_{TR} (r = 0.74) and in the opposite direction Ca_{TR} (r = –0.60). The relationships between Amazon precipitation and growth-wood density, $\delta^{18}O_{TR}$ and S_{TR}-Ca_{TR} concentration tend to be more negative after 1980. The negative correlation between Amazon precipitation and wood traits was more pronounced since 2007, similar to local precipitation. The relationships between growth-wood density and S_{TR}-Ca_{TR} and local temperature, TNA and WHWO tend to be more positive after 1980. Positive relationships between $\delta^{18}O_{TR}$ and local temperature, TNA and WHWO was observed throughout the period analyzed (Fig. S8).

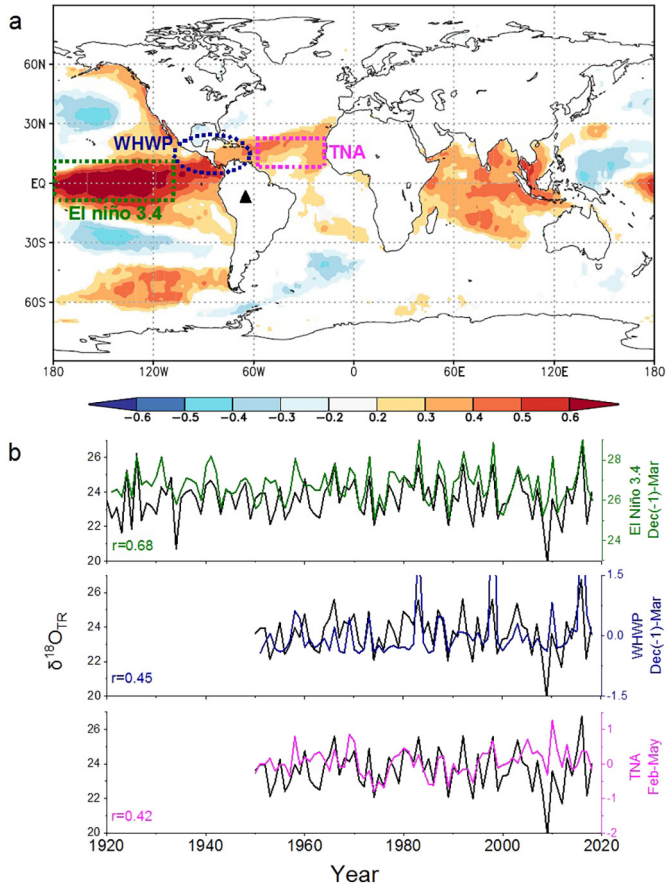

Fig. 5. a) Global spatial correlation ($p < 0.05$) between the *Cedrela fissilis* $\delta^{18}O_{TR}$ chronology and the HadISST1 1° gridded average sea surface temperatures (SST) during the rainiest months (January to March) in the sampling site (dark triangle) during the austral summer in South America. Plot computed using the KNMI-Climate Explorer. b) Association between the *Cedrela fissilis* $\delta^{18}O_{TR}$ with SST anomalies of El Niño/Southern Oscillation (El Niño 3.4; prior December–March), Western Hemisphere Warm Pool (WHWP; prior December–March) and Tropical Northern Atlantic (TNA; February–May).

4. Discussion

For the first time, a set of multiproxy chronologies from a single location has been generated from trees located in the southern Amazon basin, which is exposed to a very pronounced rainy seasonality. Specifically, the *Cedrela fissilis* collection on the study region has already provided a well dated chronology of approximately 170 years with annual periodicity validated by ^{14}C analyses (Santos et al., 2021). Here, exploratory reconstructions of local and regional precipitation, local drought intensity and global SST anomalies are presented based on tree-ring records of growth, wood density, $\delta^{18}O$ and chemical concentrations generated with Jamari *Cedrela fissilis* samples.

4.1. Climatic reconstruction based on novel wood traits from southern Amazonian trees

Previous studies in the region reported chronologies with timespans ranging from 130 to 470 years using tree ring-width (Brienen and Zuidema, 2005; Lopez et al., 2017) and stable isotope ($\delta^{13}C$ and $\delta^{18}O$) records (Baker et al., 2016; Baker et al., 2015; Brienen et al., 2012; Jenkins, 2009). These chronologies showed strong correlations with local precipitation and regional Amazon rainfall for months of the summer wet season. In the present study, the reconstructions with different wood traits that achieved the highest % of explained variance accounted for 42 % of local precipitation variability, 60 % of Amazon-wide rainfall variability, 30 % of drought intensity (P-PET) variability and 57 % of SST anomalies variability. These results aligned to previous studies from South America that explained between 35 and 68 % of the total variance of precipitation (e.g. Granato-Souza et al., 2018; Humanes-Fuente et al., 2020; Lopez et al., 2017; Pereira et al., 2018; Pucha-Cofrep et al., 2015).

In the southern Amazon region, >75 % of the average annual precipitation occurs during the 6-month rainy season from October to March (Lopez et al., 2017). The $\delta^{18}O_{TR}$ record reflect very well local precipitation variability during this rainy season showing high correlations from October to February, as well as a strong remarkable association to Amazon-wide rainfall for nearly the entire wet season (November to March). In contrast, the growth and wood density records showed strong correlations with local wet season precipitation, mainly from February to May, extending his sensitivity to the beginning of the dry season.

In addition, the RW and $\delta^{18}O_{TR}$ records were also proven to be a useful to reconstruct P-PET variability in dry-seasonal moist tropical areas. The potential use of these records in dry-seasonal moist tropical areas is relevant to place in a long-term context the observed changes in hydroclimatic variability from 1980s onwards (Fig. 1c) across the whole Amazon basin (Corlett, 2011; Marengo et al., 2009, 2011), but mainly affecting the southern region exposed to extreme drought events (Chai et al., 2021; Lovejoy and Nobre, 2018; Poulter et al., 2010). This drought conditions are expected to intensify in the immediate future due to continued deforestation of the Amazon and surrounding tropical forests (Nobre et al., 2016; Oliveira et al., 2013). Furthermore, increases in mean annual temperature close to 0.7 °C during the last four decades (Marengo et al., 2018) are a matter of rising concern for the associated increases in evapotranspiration that would impact tree physiology, growth and mortality, and thus forest structure and dynamics (Schöngart et al., 2021) with implications in global water and carbon cycles (Brienen et al., 2020).

A strong signal of precipitation was reflected by the S_{TR} record during the transition between the current dry season and the beginning of the next rainy seasons (August to October). S is a mobile element and its mainly distributed in the axial parenchyma, radial parenchyma and around the pores of *Cedrela fissilis* (Ortega Rodriguez et al., 2022). Seasonal variations and environmental conditions such as S availability from the soil and the atmosphere, mycorrhization and extreme events of heat, cold and drought affect S nutrition (Herschbach and Rennenberg, 2001). We assume that the first recharge of S in the xylem occurs just before the growth period when the formation of the marginal parenchyma is completed. Then S is discharged to be used in the protein synthesis that will allow the growth of leaves and other young parts of the tree (Herschbach and Rennenberg, 2001). Alternatively, S can be carried into the phloem, when the reduced S consumption of young leaves exceeds their own demand for growth and development (Hartmann et al., 2000), for later reallocation into the xylem storage tissues or the root at the beginning of the next growing season when the sap flow increases (Herschbach and Rennenberg, 2001). This may explain the significant correlation of S concentrations with the beginning of the next rainy season.

The Ca_{TR} record showed strong correlations with the precipitation of the beginning of the rainy season (September to October). Ca, an immobile element, is distributed in all cells of the growth ring, but mainly around the vessels, with a higher concentration in the transition from latewood to earlywood in the case of *Cedrela fissilis* (Ortega Rodriguez et al., 2022). Therefore, Ca is mainly deposited in the cell walls and is essential for the onset of cambial reactivation and cell division at the beginning of the growth season (Fromm, 2010), which explains the strong correlation with precipitation from September to October. These correlations between trace element and seasonal rainfall outlines the potential of dendrochemical data for paleoclimate applications in the tropical regions.

Our study also reported a strong association between $\delta^{18}O_{TR}$ and S_{TR} records and local temperature during the wet seasons (Fig. S5). However, caution is needed interpreting these results considering that temperature is not expected to be dominant driver of $\delta^{18}O_{TR}$ interannual variability in the Amazon (Baker et al., 2016; Cintra et al., 2021) as oppose as in higher latitudes (e.g. Field et al., 2022). This association may arise as an artifact

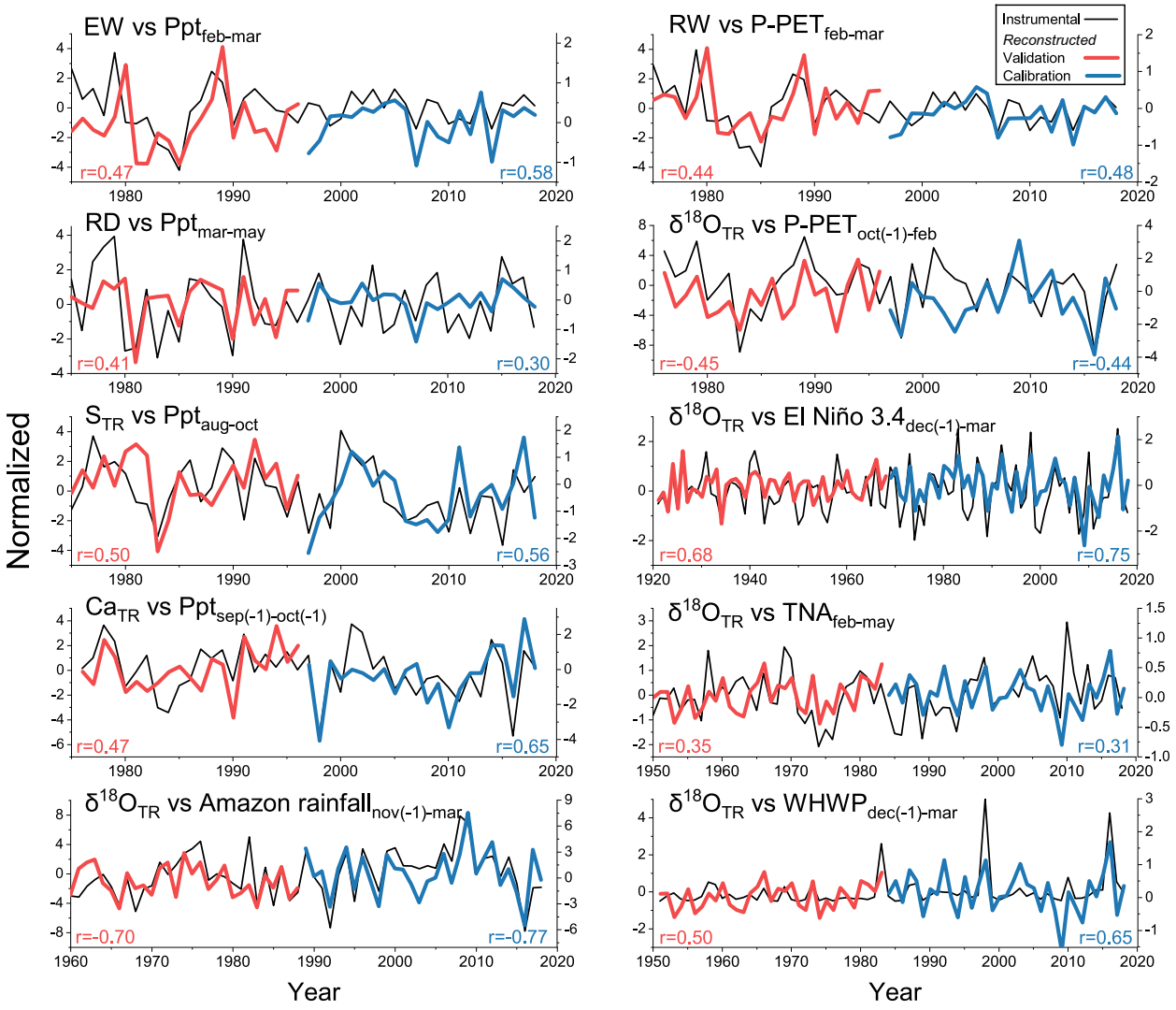

Fig. 6. The selected wood trait chronologies (black lines) for testing reconstruction models were tree-ring width (RW), earlywood width (EW), ring wood density (RD), $\delta^{18}O_{TR}$, and concentrations of Sulfur (S_{TR}) and Calcium (Ca_{TR}). The instrumental data that served as a target to reconstruct were precipitation totals (Ppt), Amazon-wide rainfall total, difference between precipitation and evapotranspiration (P-PET) and sea surface temperature (SST) anomalies of El Niño/Southern Oscillation (El Niño 3.4), Tropical Northern (TNA), and Western Hemisphere Warm Pool (WHWP). The wood trait chronologies were calibrated (C) and validated (V) against the instrumental data (C: blue lines; V: red lines) for Precipitation and P-PET totals for C (1997–2018) and V (1975–1996), Amazon-wide rainfall totals for C (1989–2018) and V (1960–1988), El Niño 3.4 mean for C (1969–2018) and V (1921–1968), and TNA and WHWP mean for C (1984–2018) and V (1950–1983). Months indicated as (−1) correspond to the month of the prior year.

of covariations between large-scale external controls (e.g. ENSO) and climatic conditions, which disappear once the temperature trend is removed (Cintra et al., 2021). High co-variance between precipitation and temperature in these latitudes, in particular during the wet season, have been also pointed out as some of reasons for the temperature signial in the $\delta^{18}O_{TR}$ record (Rodriguez-Caton et al., 2021). Regarding the negative

Table 2
Calibration and verification statistics for the tested reconstruction models of local (Precipitation, Ppt; difference between precipitation and evapotranspiration, P-PET), regional (Amazon rainfall) and global (monthly sea surface temperature anomalies of Tropical Northern, TNA; Western Hemisphere Warm Pool, WHWP; and El Niño/Southern Oscillation, El Niño 3.4) climatic variables, where r / r_{adj} are the correlation coefficient; R^2 / R^2_{adj} are the coefficient of determination adjusted for loss of degrees of freedom; DW is the Durbin-Watson test; RE is the reduction of error and RMSEv is the root mean squared error of validation.

Variable reconstructed	Predictors (Chronology)	Calibration period	r / r_{adj}	R^2 / R^2_{adj}	DW	RE	$RMSE_v$	Reconstructed period
$Ppt_{feb\text{-}mar}$	EW	1997–2018	0.58 / 0.47	0.34 / 0.20	1.836	0.185	0.208	1975–1996
$Ppt_{mar\text{-}may}$	RD	1997–2018	0.30 / 0.41	0.10 /0.26	2.142	0.172	0.042	1975–1996
$Ppt_{aug\text{-}oct}$	S	1997–2018	0.56 /0.50	0.31 / 0.18	2.202	0.196	0.718	1975–1996
$Ppt_{sep(-1)\text{-}oct(-1)}$	Ca	1997–2018	0.65 / 0.47	0.42 / 0.17	1.654	−1.194	0.489	1975–1996
Amazon $rainfall_{nov(-1)\text{-}mar}$	$\delta^{18}O_{TR}$	1989–2018	0.77 / 0.70	0.60 / 0.29	0.968	0.38	0.768	1960–1988
$P\text{-}PET_{feb\text{-}mar}$	RW	1997–2018	0.48 / 0.44	0.30 / 0.19	2.244	0.16	0.243	1975–1996
$P\text{-}PET_{oct(-1)\text{-}feb}$	$\delta^{18}O_{TR}$	1997–2018	0.44 / 0.45	0.20 / 0.28	1.971	0.158	1.333	1975–1996
El Niño $3.4_{dec(-1)\text{-}mar}$	$\delta^{18}O_{TR}$	1969–2018	0.75 / 0.68	0.57 / 0.32	1.811	0.149	0.077	1921–1968
$TNA_{feb\text{-}may}$	$\delta^{18}O_{TR}$	1984–2018	0.31 /0.35	0.10 / 0.18	1.236	0.141	0.122	1950–1983
$WHWP_{dec(-1)\text{-}mar}$	$\delta^{18}O_{TR}$	1984–2018	0.65 / 0.50	0.30 / 0.17	1.893	−0.085	0.383	1950–1983

S_{TR}-temperature correlations in the wet period, it is possible that with high temperatures the translocation of S increases, in its stored form as glutathione (GSH), from the xylem to the growing parts of the shoot and unloaded in the leaves to play a defense function against heat stress. GSH is an S-stored and transported form in xylem tissues, is involved in the regulation of S nutrition, and is essential for the plant's defense system in stress situations (Herschbach and Rennenberg, 2001; Ihsan et al., 2019). Accumulation of GSH in plant cells is triggered by heat and drought stress, becoming oxidized (GSSG) and maintaining optimal cellular redox and biochemical functions within the plant cells (Ihsan et al., 2019). The effect of temperature conditioning the translocation of S and its decrease in the xylem tissues must be verified in other *Cedrela* populations and other tropical species adapted to hotter and drier environments, since previous studies in different deciduous trees in temperate regions showed contrasting results in GSH mobilization (see Herschbach and Rennenberg, 2001).

4.2. Global modes recorded in tree-ring wood traits

Summer precipitation in the southern Amazon basin is influenced by interactions between the SAMS and incursions of cold and dry extratropical air (Hurley et al., 2015; Lopez et al., 2017; Marengo and Rogers, 2001). The 20 % of the SASM precipitation variability is influenced by ENSO, which induces significant atmospheric circulation anomalies over tropical South America (Foley et al., 2002; Garreaud et al., 2009; Vuille and Werner, 2005). The strong positive correlations between the *Cedrela fissilis* $\delta^{18}O_{TR}$ chronology and SST in the central equatorial Pacific (El Niño 3.4 region) observed during the austral summer (mainly from prior December to March) in our study (Fig. 5) agreed with the signal observed with the *Cedrela odorata* $\delta^{18}O_{TR}$ chronology located at northern Bolivia (11°24′ S, 68°43′ W; Brienen et al., 2012), and also with four *Polylepis tarapacana* $\delta^{18}O_{TR}$ records from the Altiplano above 4000 m.a.s.l. (Rodriguez-Caton et al., 2022). This indicates that the warmer the tropical Pacific SST, the higher the $\delta^{18}O_{TR}$ records because $\delta^{18}O$. Our results also showed that the ENSO phase (El Niño 3.4) induced a significant increase in *Cedrela fissilis* wood density and a significant decrease in radial growth during the wet season (particularly from prior September to prior October and from February to May, respectively), while Ca_{TR} concentrations also decrease albeit not significantly (Fig. S7).

The ENSO oscillations showed wavelengths from 2 to 8 years (Deser et al., 2010) that we also found in the wood trait chronologies (Fig. S3) RW and LWD (1850 to 1950), EW, LW, RD and EWD (1950 onwards), $\delta^{18}O_{TR}$ (1980 onwards) and Ca_{TR} (1940 to 2000). Nevertheless, the ENSO influence has not always been dominant during the last century in neotropical regions (Brienen et al., 2012; Crispín-DelaCruz et al., 2022; Humanes-Fuente et al., 2020; Jenkins, 2009; Lopez et al., 2017). In particular, the southern Amazon precipitation appears to be less sensitive to ENSO events than the northern region (Jenkins, 2009; Lopez et al., 2017), mainly during the middle of the century (1930–1970) (Brienen et al., 2012; Labat et al., 2004). Furthermore, the $\delta^{18}O_{TR}$-ENSO correlations in the southern Amazon are weaker during the middle of the century and stronger during the beginning and at the end of the last century (Figs. S3 and 5; Brienen et al., 2012). The lower $\delta^{18}O_{TR}$-ENSO association during the middle of the century coincides with periods of lower variance in the Southern Oscillation Index (the atmospheric branch of El Niño) (Torrence and Webster, 1999). In contrast, the stronger $\delta^{18}O_{TR}$-ENSO correlations during the end of the last century coincide with warmer periods of the Pacific Decadal Oscillation (PDO, dominated from 1925 to 1946 and from 1977 to 2000), which resulted in more frequent El Niño events (Mantua and Hare, 2002) and decreased rainfall in the Amazon Basin (Foley et al., 2002; Liebmann and Marengo, 2001).

Aside from ENSO, a second driver behind summer precipitation variability in South America, and therefore in the Amazon basin, is related to Atlantic SSTs variability that exhibited decadal and multidecadal oscillations (Chiessi et al., 2009; Marengo, 2004; Nobre and Shukla, 1996; Zhou and Lau, 2001). Our results showed a positive association of the $\delta^{18}O_{TR}$ chronology with TNA (decadal) during the end of summer precipitation and at the beginning of dry season from February to May and with AMO (multidecal) from March to June, respectively (Fig. S7). Jenkins (2009) and Brienen et al. (2012) reported similar high $\delta^{18}O_{TR}$ and TNA correlations during the rainy season. The positive phase of AMO also induced more growth (significantly for LW) and higher wood density (significantly for RD and EWD) from June to August (Fig. S7). The TNA negatively affected S and Ca concentrations during March to August (although not significantly), while TSA positively influenced wood density (significantly for RD and EWD) during July to August (Fig. S7). It is likely that the decadal to multidecal oscillation of the Atlantic SST is the signal recorded in RW (1850 to 1920), EWD (1960 onwards), LW, RD and LWD (1850 to 1960), EW and $\delta^{18}O_{TR}$ (1960 onwards), S_{TR} and Ca_{TR} (1910 to 2000) (Fig. S3).

The AMO also plays a significant role in modulating multidecadal SAMS variability (Chiessi et al., 2009). Indeed after 1950 the multidecadal component of AMO variability increased substantially in the Southern Amazon basin (Lopez et al., 2017), which coincided with more intense and prolonged droughts and floods (Marengo and Espinoza, 2016). The TNA signatures in the $\delta^{18}O_{TR}$ chronologies (Figs. S3, S7, 5; Cintra et al., 2021; Jenkins, 2009) may be related to March–May rainfall variability over northeast South America (NSA). There is a north-south dipole-like pattern in precipitation associated to variations in the ITCZ shifts produced by the combined effect of Pacific and Atlantic SST anomalies (Rodríguez-Fonseca et al., 2009), which increased after 1970s (Torralba et al., 2015) and extended to the southern Amazon basin (12°S and 60°W). The TNA signatures may be also explained by the northward ITCZ shift (i.e. resulting in dry conditions in southeastern Amazon), which may be associated to an increase in the SST gradient from the tropical to the subpolar North Atlantic due to tropical SST warming and North Atlantic SST cooling with ice melt (Hilker et al., 2014; Malhi et al., 2008).

Besides the ENSO and Atlantic SSTs influences, the $\delta^{18}O_{TR}$ chronology detected signatures (mainly after 1980) of the SST of the intra-American region (WHWP) from December to March (Figs. 5, S7). The WHWP thermal variability is reported to have an important influence on the modifications in the subsidiary movements of the southern (Hadley cells) and zonal (Walker cells) atmospheric circulations that can influence the occurrence of more or less rainy periods in the NSA region (Reboita and Santos, 2015; Wang and Enfield, 2003; Wang and Enfield, 2001). Although there are still few studies about the magnitude and extension of WHWP influences in the NSA region, strong associations between anomalous November–May warming of WHWP and less growth of *Cedrela odorata* from a seasonally dry tropical forest in northeastern Brazil were reported (Menezes et al., 2022).

4.3. Stability of the climate signal in wood trait chronologies

Since the middle of the last century, climate and atmospheric changes have been recorded across South America, mainly related to changes in SASM, when the Tropical Low-Pressure Belt (TLPB) reaches its southernmost latitudinal position (Ancapichún et al., 2021; Espinoza et al., 2019; Gloor et al., 2015; Gloor et al., 2013; Morales et al., 2020; Segura et al., 2020). In seasonal dry forests of the southern Amazon region the increase in temperature and evapotranspiration in recent decades has translated into more prolonged droughts (Chai et al., 2021; Lovejoy and Nobre, 2018). In particular, at our study site JNF, less rainy and drier years during the 1976–2018 period, are associated with less rainy years Amazon-wide and higher local temperatures together with warm Pacific and Atlantic SSTs (Table S2). The climate dynamics associated to local (e.g. precipitation, temperature and evapotranspiration) and global (e.g. STTs anomalies) variables and their associated effects such as drought events, can be reflected in the long-term variability of tree-ring records (Figs. 3, S3 and S8; Lopez et al., 2017). Our temporally correlation analysis suggests that *Cedrela. fissilis* experiences changes in relation to climate and atmospheric variability from 1980 onwards (Fig. S8). The negative and positive trend of the relationships of the wood traits with the local precipitation and temperature (and SST anomalies), respectively, can be related to more frequent (one extreme event every ~4.5 years) and severe droughts occurring in

almost all continents (Morales et al., 2020), that became increasingly intense since 2000 in the Amazonian Andes of Peru (Humanes-Fuente et al., 2020). Furthermore, in the Amazon basin, ENSO episodes (El Niño 3.4) or warm Atlantic conditions (TNA, WHWP and AMO) are the main drivers of local temperature increases (Marengo et al., 2018) and can be linked to the most of the droughts recorded in the last century (Jimenez et al., 2021; Marengo et al., 2016).

The decrease in the strength of wood traits-precipitation associations and the increase in the strength of of wood traits-temperature correlations (mainly 1998 onwards) may suggest that trees in the southern Amazon region are adjusting their growth (also nutritional and physiological traces) to water availability and becoming increasingly sensitive to local temperature changes and SST anomalies. Drastic changes in the wood traits responses to climate variables may become more frequent due to the increase in drought episodes, which may imply drought resistance strategies implemented by trees (Camarero et al., 2020; Mendivelso et al., 2014). These drought resistance strategies can translate into adaptation processes or trade-offs over time between tree growth, hydraulic efficiency, mechanical safety (Islam et al., 2019; Janssen et al., 2019; Lachenbruch and Mcculloh, 2014) or nutrient balance (Hevia et al., 2019).

5. Conclusions

This study demostrated the feasibility to reconstruct annual, decadal and multidecadal variability of local precipitation and temperature, Amazon-wide precipitation and global modes (ENSO, TNA, WHWP and AMO) using multi-proxy tree-ring records of wood traits. Ring width, wood density, $\delta^{18}O_{TR}$ and concentration of Sulfur and Calcium annual-resolved tree-ring records generated here provided complementary information on the climate dynamics in the southern Amazon region. While ring-width, wood density and chemical concentrations better express the local climate variability, the $\delta^{18}O_{TR}$ record reflects better climate information at regional and global levels.

In the southern Amazon region, currently increasing drought conditions have been observed mainly caused by a later onset of the rainy season (Marengo et al., 2018). Regarding future scenarios, a more pronounce temperature increase is expected in southern Amazonia due to increases in SST anomalies (IPCC, 2021). In this context, our multi proxy approach provide new records with accurate climate sensitivity for local and regional forecasting of climatic processes.

CRediT authorship contribution statement

Conceptualization: DROR, RSS, FAR, MTF. Methodology: DROR, RSS, AH, DGS, BC, BH, GAP. Resources: RSS, AH, BC, MTF. Sample collection and preparation: DROR, BH. Sample analysis: DROR, RSS, AH, BH. Data analysis: DROR, RSS, DGS, GAP. Writing: DROR, RSS, AH, FAR, MTF. Reviewing: DGS, BH, BC, LAH, GAP. Editing: DROR, RSS, LAH. Supervision: FAR, MTF.

Data availability

Data will be made available on request.

Declaration of competing interest

The authors declare that the research was conducted in the absence of any commercial or financial relationships that could be construed as a potential conflict of interest.

Acknowledgements

We thank the Wood Anatomy and Tree-Ring Laboratory (LAIM) (FAPESP project: 2009/53951-7), Department of Forest Sciences, Luiz de Queiroz College of Agriculture (ESALQ). This research was supported by the Post-Graduate Program of Forest Resources (ESALQ-USP, Brazil), and FAPESP grants 2020/04608-7, 2018/22914-8 and 2017/50085-3. RSS was supported by VULBOS project (UPO-1263216), VURECLIM (P20_00813) and AH by PinCaR project (UHU-1266324) both by FEDER Funds, Andalusia Regional Government, Consejería de Economía, Conocimiento, Empresas y Universidad 2014-2020. RSS and AH were also supported by EQC2018-004821-P and IE19_074 UPO projects cofunded by Spanish "Plan Estatal de Investigación Científica y Técnica y de Innovación 2017-2020" and "Plan Andaluz de Invetigación, Desarrollo e Innovación (PAIDI 2020)", respectively. GAP was supported by CAPES (grant # 88887.199858/2018-00) in the National Academic Cooperation Program in the Amazon. Additional thanks to the logging company AMATA for their assistance in the field work.

Appendix A. Supplementary data

Supplementary data to this article can be found online at https://doi.org/10.1016/j.scitotenv.2023.162064.

References

Agudelo, J., Arias, P.A., Vieira, S.C., Martínez, J.A., 2019. Influence of longer dry seasons in the southern Amazon on patterns of water vapor transport over northern South America and the Caribbean. Clim. Dyn. 52, 2647–2665. https://doi.org/10.1007/s00382-018-4285-1.

Ancapichún, S., De Pol-Holz, R., Christie, D.A., Santos, G.M., Collado-Fabbri, S., Garreaud, R., Lambert, F., Orfanoz-Cheuquelaf, A., Rojas, M., Southon, J., Turnbull, J.C., Creasman, P.P., 2021. Radiocarbon bomb-peak signal in tree-rings from the tropical Andes register low latitude atmospheric dynamics in the southern hemisphere. Sci. Total Environ. 774, 145126. https://doi.org/10.1016/j.scitotenv.2021.145126.

Baker, J.C.A., Gloor, M., Spracklen, D.V., Arnold, S.R., Tindall, J.C., Clerici, S.J., Leng, M.J., Brienen, R.J.W., 2016. What drives interannual variation in tree ring oxygen isotopes in the Amazon? Geophys. Res. Lett. 43, 11831–11840. https://doi.org/10.1002/2016GL071507.

Baker, J.C.A., Hunt, S.F.P., Clerici, S.J., Newton, R.J., Bottrell, S.H., Leng, M.J., Heaton, T.H.E., Helle, G., Argollo, J., Gloor, M., Brienen, R.J.W., 2015. Oxygen isotopes in tree rings show good coherence between species and sites in Bolivia. Glob. Planet. Change 133, 298–308. https://doi.org/10.1016/j.gloplacha.2015.09.008.

Balouet, J.C., Smith, K.T., Vroblesky, D., Oudijk, G., 2009. Use of dendrochronology and dendrochemistry in environmental forensics: does it meet the daubert criteria? Environ Forensics 10, 268–276. https://doi.org/10.1080/15275920903347545.

Barichivich, J., Gloor, E., Peylin, P., Brienen, R.J.W., Schöngart, J., Espinoza, J.C., Pattnayak, K.C., 2018. Recent intensification of Amazon flooding extremes driven by strengthened Walker circulation. Sci. Adv. 4. https://doi.org/10.1126/sciadv.aat8785.

Björklund, J., von Arx, G., Nievergelt, D., Wilson, R., Van den Bulcke, J., Günther, B., Loader, N.J., Rydval, M., Fonti, P., Scharnweber, T., Andreu-Hayles, L., Büntgen, U., D'Arrigo, R., Davi, N., De Mil, T., Esper, J., Gärtner, H., Geary, J., Gunnarson, B.E., Hartl, C., Hevia, A., Song, H., Janecka, K., Kaczka, R.J., Kirdyanov, A.V., Kochbeck, M., Liu, Y., Meko, M., Mundo, I., Nicolussi, K., Oelkers, R., Pichler, T., Sánchez-Salguero, R., Schneider, L., Schweingruber, F., Timonen, M., Trouet, V., Van Acker, J., Verstege, A., Villalba, R., Wilmking, M., Frank, D., 2019. Scientific merits and analytical challenges of tree-ring densitometry. Rev. Geophys. 57, 1224–1264. https://doi.org/10.1029/2019RG000642.

Boninsegna, J.A., Argollo, J., Aravena, J.C., Barichivich, J., Christie, D., Ferrero, M.E., Lara, A., Le Quesne, C., Luckman, B.H., Masiokas, M., Morales, M., Oliveira, J.M., Roig, F., Srur, A., Villalba, R., 2009. Dendroclimatological reconstructions in South America: a review. Palaeogeogr. Palaeoclimatol. Palaeoecol. 281, 210–228. https://doi.org/10.1016/j.palaeo.2009.07.020.

Brienen, R.J.W., Caldwell, L., Duchesne, L., Voelker, S., Barichivich, J., Baliva, M., Ceccantini, G., Di Filippo, A., Helama, S., Locosselli, G.M., Lopez, L., Piovesan, G., Schöngart, J., Villalba, R., Gloor, E., 2020. Forest carbon sink neutralized by pervasive growth-lifespan trade-offs. Nat. Commun. 11. https://doi.org/10.1038/s41467-020-17966-z.

Brienen, R.J.W., Helle, G., Pons, T.L., Guyot, J.-L., Gloor, M., 2012. Oxygen isotopes in tree rings are a good proxy for Amazon precipitation and El Niño-southern oscillation variability. Proc. Natl. Acad. Sci. 109, 16957–16962. https://doi.org/10.1073/PNAS.1205977109.

Brienen, R.J.W., Schöngart, J., Zuidema, P.A., 2016. Tree rings in the tropics: Insights into the ecology and climate sensitivity of tropical trees. In: Goldstein, G., Santiago, L. (Eds.), Tropical Tree Physiology. Springer, Cham https://doi.org/10.1007/978-3-319-27422-5_20.

Brienen, R.J.W., Zuidema, P.A., 2005. Relating tree growth to rainfall in bolivian rain forests: a test for six species using tree ring analysis. Oecologia 146, 1–12. https://doi.org/10.1007/s00442-005-0160-y.

Briffa, K.R., Osborn, T.J., Schweingruber, F.H., Jones, P.D., Shiyatov, S.G., Vaganov, E.A., 2002. Tree-ring width and density data around the northern hemisphere: part 2, spatio-temporal variability and associated climate patterns. The Holocene 12, 759–789. https://doi.org/10.1191/0959683602hl588rp.

Callède, J., Cochonneau, G., Alves, F.V., Guyot, J.-L., Guimarães, V.S., De Oliveira, E., 2010. Les apports en eau de l'Amazone à l'Océan Atlantique. Rev. des Sci. l'eau 23, 247–273. https://doi.org/10.7202/044688ar.

Camarero, J.J., Mendivelso, H.A., Sanchez-salguero, R., 2020. How past and future climate and drought drive radial-growth variability of three tree species in a bolivian tropical

dry Forest. In: Pompa-García, M., Camarero, J.J. (Eds.), Latin American Dendroecology. Springer, Cham, pp. 121–140 https://doi.org/10.1007/978-3-030-36930-9_7.
Chai, Y., Martins, G., Nobre, C., Von Randow, C., Chen, T., Dolman, H., 2021. Constraining amazonian land surface temperature sensitivity to precipitation and the probability of forest dieback. npj Clim. Atmos. Sci. 4. https://doi.org/10.1038/s41612-021-00162-1.
Chiessi, C.M., Mulitza, S., Pätzold, J., Wefer, G., Marengo, J.A., 2009. Possible impact of the Atlantic multidecadal oscillation on the south american summer monsoon. Geophys. Res. Lett. 36. https://doi.org/10.1029/2009GL039914.
Cintra, B., Gloor, M., Boom, A., Schöngart, J., Locosselli, G., Brienen, R., 2019. Contrasting controls on tree ring isotope variation for Amazon floodplain and terra firme trees. Tree Physiol. 39, 845–860. https://doi.org/10.1093/TREEPHYS/TPZ009.
Cintra, B.B.L., Gloor, M., Boom, A., Schöngart, J., Baker, J.C.A., Cruz, F.W., Clerici, S., Brienen, R.J.W., 2021. Tree - ring oxygen isotopes record a decrease in Amazon dry season rainfall over the past 40 years. Clim. Dyn. https://doi.org/10.1007/s00382-021-06046-7.
Collini, E.A., Berbery, E.H., Barros, V.R., Pyle, M.E., 2008. How does soil moisture influence the early stags of the South American monsoon? J. Clim. 21, 195–213. https://doi.org/10.1175/2007JCLI1846.1.
Cook, E., Krusic, P., 2005. Program ARSTAN: a tree-ring standardiza- tion program based on detrending and autoregressive time series modeling, with interactive graphics. Manuscr. file, Tree-Ring Lab. Lamont Doherty Earth Obs. Columbia Univ. Palisades.
Cook, E.R., 1985. A Time Series Approach to Tree-ring Standardisation. University of Arizona.
Cook, E.R., Briffa, K.R., Jones, P.D., 1994. Spatial regression methods in dendroclimatology: a review and comparison of two techniques. Int. J. Climatol. 14, 379–402. https://doi.org/10.1002/joc.3370140404.
Cook, E.R., Pederson, N., 2011. Uncertainty, Emergence, and Statistics in Dendrochronology. Springer, Dordrecht, pp. 77–112 https://doi.org/10.1007/978-1-4020-5725-0_4.
Corlett, R.T., 2011. Impacts of warming on tropical lowland rainforests. Trends Ecol. Evol. https://doi.org/10.1016/j.tree.2011.06.015.
Crispín-DelaCruz, D.B., Morales, M.S., Andreu-Hayles, L., Christie, D.A., Guerra, A., Requena-Rojas, E.J., 2022. High ENSO sensitivity in tree rings from a northern population of polylepis tarapacana in the peruvian Andes. Dendrochronologia 71. https://doi.org/10.1016/j.dendro.2021.125902.
Croudace, I.W., Rindby, A., Rothwell, R.G., 2006. ITRAX: description and evaluation of a new multi-function X-ray core scanner. Geol. Soc. Spec. Publ. 267, 51–63. https://doi.org/10.1144/GSL.SP.2006.267.01.04.
Cutter, B.E., Guyette, R.P., 1993. Anatomical, chemical, and ecological factors affecting tree species choice in dendrochemistry studies. J. Environ. Qual. 22, 611. https://doi.org/10.2134/jeq1993.00472425002200030028x.
Cybis Electronic, 2013. CDendro and CooRecorder V.7.7.
Della Libera, M.E., Novello, V.F., Cruz, F.W., Orrison, R., Vuille, M., Maezumi, S.Y., de Souza, J., Cauhy, J., Campos, J.L.P.S., Ampuero, A., Utida, G., Stríkis, N.M., Stumpf, C.F., Azevedo, V., Zhang, H., Edwards, R.L., Cheng, H., 2022. Paleoclimatic and paleoenvironmental changes in amazonian lowlands over the last three millennia. Quat. Sci. Rev. 279, 107383. https://doi.org/10.1016/J.QUASCIREV.2022.107383.
Deser, C., Alexander, M.A., Xie, S.P., Phillips, A.S., 2010. Sea surface temperature variability: patterns and mechanisms. Annu. Rev. Mar. Sci. 2, 115–143. https://doi.org/10.1146/annurev-marine-120408-151453.
Dünisch, O., 2005. Influence of the El-niño southern oscillation on cambial growth of Cedrela fissilis vell. In tropical and subtropical Brazil. J. Appl. Bot. Food Qual. 79, 5–11.
Espinoza, J.C., Ronchail, J., Marengo, J.A., Segura, H., 2019. Contrasting north-south changes in Amazon wet-day and dry-day frequency and related atmospheric features (1981–2017). Clim. Dyn. 52, 5413–5430. https://doi.org/10.1007/s00382-018-4462-2.
Fairchild, I.J., Loader, N.J., Wynn, P.M., Frisia, S., Thomas, P.A., Lageard, J.G.A., De Momi, A., Hartland, A., Borsato, A., La Porta, N., Susini, J., 2009. Sulfur fixation in wood mapped by synchrotron x-ray studies: implications for environmental archives. Environ. Sci. Technol. 43, 1310–1315. https://doi.org/10.1021/es8029297.
Field, R.D., Andreu-Hayles, L., D'arrigo, R.D., Oelkers, R., Luckman, B.H., Morimoto, D., Boucher, E., Gennaretti, F., Hermoso, I., Lavergne, A., Levesque, M., 2022. Tree-ring cellulose δ18O records similar large-scale climate influences as precipitation δ18O in the Northwest Territories of Canada. Clim. Dyn. 58, 759–776. https://doi.org/10.1007/s00382-021-05932-4.
Foley, J.A., Botta, A., Coe, M.T., Costa, M.H., 2002. El Niño-Southern oscillation and the climate, ecosystems and rivers of Amazonia. Global Biogeochem. Cycles 16. https://doi.org/10.1029/2002GB001872 79-1–79-20.
Frank, D., Esper, J., Cook, E.R., 2007. Adjustment for proxy number and coherence in a large-scale temperature reconstruction. Geophys. Res. Lett. 34. https://doi.org/10.1029/2007GL030571.
Fritts, H.C., 1976. Tree Rings and Climate. Academic Press.
Fromm, J., 2010. Wood formation of trees in relation to potassium and calcium nutrition. Tree Physiol. 30, 1140–1147. https://doi.org/10.1093/treephys/tpq024.
Garreaud, R.D., Vuille, M., Compagnucci, R., Marengo, J., 2009. Present-day south american climate. Palaeogeogr. Palaeoclimatol. Palaeoecol. 281, 180–195. https://doi.org/10.1016/j.palaeo.2007.10.032.
Gärtner, H., Schweingruber, F.H., 2013. Microscopic Preparation Techniques for Plant Stem Analysis. Kessel.
Gloor, M., Barichivich, J., Ziv, G., Brienen, R., Schöngart, J., Peylin, P., Ladvocat Cintra, B.B., Feldpausch, T., Phillips, O., Baker, J., 2015. Recent Amazon climate as background for possible ongoing and future changes of Amazon humid forests. Glob. Biogeochem. Cycles 29, 1384–1399. https://doi.org/10.1002/2014GB005080.
Gloor, M., Brienen, R.J.W., Galbraith, D., Feldpausch, T.R., Schöngart, J., Guyot, J.L., Espinoza, J.C., Lloyd, J., Phillips, O.L., 2013. Intensification of the Amazon hydrological cycle over the last two decades. Geophys. Res. Lett. 40, 1729–1733. https://doi.org/10.1002/grl.50377.
Gonçalves, J.Q., Durgante, F.M., Wittmann, F., Piedade, M.T.F., Ortega Rodriguez, D.R., Tomazello, M., Parolin, P., Schöngart, J., 2021. Minimum temperature and evapotranspiration in central amazonian floodplains limit tree growth of Nectandra amazonum (lauraceae). Trees https://doi.org/10.1007/s00468-021-02126-7.
Granato-Souza, D., Stahle, D.W., Barbosa, A.C., Feng, S., Torbenson, M.C.A., de Assis Pereira, G., Schöngart, J., Barbosa, J.P., Griffin, D., 2018. Tree rings and rainfall in the equatorial Amazon. Clim. Dyn. 52, 1857–1869. https://doi.org/10.1007/s00382-018-4227-y.
Granato-Souza, D., Stahle, D.W., Torbenson, M.C.A., Howard, I.M., Barbosa, A.C., Feng, S., Fernandes, K., Schöngart, J., 2020. Multidecadal changes in wet season precipitation totals over the eastern Amazon. Geophys. Res. Lett. 47, 1–9. https://doi.org/10.1029/2020gl087478.
Guan, K., Pan, M., Li, H., Wolf, A., Wu, J., Medvigy, D., Caylor, K.K., Sheffield, J., Wood, E.F., Malhi, Y., Liang, M., Kimball, J.S., Saleska, S.R., Berry, J., Joiner, J., Lyapustin, A.I., 2015. Photosynthetic seasonality of global tropical forests constrained by hydroclimate. Nat. Geosci. 8, 284–289. https://doi.org/10.1038/ngeo2382.
Harris, I., Osborn, T.J., Jones, P., Lister, D., 2020. Version 4 of the CRU TS monthly high-resolution gridded multivariate climate dataset. Sci. Data 7, 109. https://doi.org/10.1038/s41597-020-0453-3.
Hartmann, T., Mult, S., Suter, M., Rennenberg, H., Herschbach, C., 2000. Leaf age-dependent differences in Sulphur assimilation and allocation in poplar (Populus tremula x P. alba) leaves. J. Exp. Bot. 51, 1077–1088. https://doi.org/10.1093/jexbot/51.347.1077.
Herschbach, C., Rennenberg, H., 2001. Sulfur nutrition of deciduous trees. Naturwissenschaften 88, 25–36. https://doi.org/10.1007/s001140000200.
Hevia, A., Sánchez-Salguero, R., Camarero, J.J., Buras, A., Sangüesa-Barreda, G., Galván, J.D., Gutiérrez, E., 2018. Towards a better understanding of long-term wood-chemistry variations in old-growth forests: a case study on ancient Pinus uncinata trees from the Pyrenees. Sci. Total Environ. 625, 220–232. https://doi.org/10.1016/j.scitotenv.2017.12.229.
Hevia, A., Sánchez-Salguero, R., Camarero, J.J., Querejeta, J.I., Sangüesa-Barreda, G., Gazol, A., 2019. Long-term nutrient imbalances linked to drought-triggered forest dieback. Sci. Total Environ. 690, 1254–1267. https://doi.org/10.1016/j.scitotenv.2019.06.515.
Hilker, T., Lyapustin, A.I., Tucker, C.J., Hall, F.G., Myneni, R.B., Wang, Y., Bi, J., De Moura, Y.M., Sellers, P.J., 2014. Vegetation dynamics and rainfall sensitivity of the Amazon. Proc. Natl. Acad. Sci. U. S. A. 111, 16041–16046. https://doi.org/10.1073/pnas.1404870111.
Holmes, R., 1983. Computer-assisted Quality Control in Tree-Ring Dating and Measurement. Tree-ring Bull.
Humanes-Fuente, V., Ferrero, M.E., Muñoz, A.A., González-Reyes, Á., Requena-Rojas, E.J., Barichivich, J., Inga, J.G., Layme-Huaman, E.T., 2020. Two centuries of hydroclimatic variability reconstructed from tree-ring records over the amazonian Andes of Peru. J. Geophys. Res. Atmos. 125, e2020JD032565. https://doi.org/10.1029/2020JD032565.
Hurley, J.V., Vuille, M., Hardy, D.R., Burns, S.J., Thompson, L.G., 2015. Cold air incursions, δ18O variability, and monsoon dynamics associated with snow days at Quelccaya Ice Cap, Peru. J. Geophys. Res. 120, 7467–7487. https://doi.org/10.1002/2015JD023323.
Ihsan, M.Z., Daur, I., Alghabari, F., Alzamanan, S., Rizwan, S., Ahmad, M., Waqas, M., Shafqat, W., 2019. Heat stress and plant development: role of Sulphur metabolites and management strategies. Acta agricScand. Sect. B Soil Plant Sci. 69, 332–342. https://doi.org/10.1080/09064710.2019.1569715.
IPCC, 2021. Climate Change 2021: The Physical Science Basis. Cambridge University Press.
Islam, M., Rahman, M., Bräuning, A., 2019. Impact of extreme drought on tree-ring width and vessel anatomical features of Chukrasia tabularis. Dendrochronologia 53, 63–72. https://doi.org/10.1016/J.DENDRO.2018.11.007.
Janssen, T.A.J., Hölttä, T., Fleischer, K., Naudts, K., Dolman, H., Thomas, J., Janssen, C.A., 2019. Wood Allocation Trade-offs Between Fiber Wall, Fiber Lumen, and Axial Parenchyma Drive Drought Resistance in Neotropical Trees. https://doi.org/10.1111/pce.13687.
Jenkins, H.S., 2009. Amazon climate reconstruction using growth rates and stable isotopes of tree ring cellulose from the Madre de Dios basin. Duke University, Peru.
Jimenez, J.C., Marengo, J.A., Alves, L.M., Sulca, J.C., Takahashi, K., Ferrett, S., Collins, M., 2021. The role of ENSO flavours and TNA on recent droughts over Amazon forests and the Northeast Brazil region. Int. J. Climatol. 41, 3761–3780. https://doi.org/10.1002/joc.6453.
Krusic, P.J., 2006. Program DPL.
Labat, D., Ronchail, J., Callede, J., Guyot, J.L., De Oliveira, E., Guimaraes, W., 2004. Wavelet analysis of Amazon hydrological regime variability. Geophys. Res. Lett. 31. https://doi.org/10.1029/2003GL018741.
Lachenbruch, B., Mcculloh, K.A., 2014. Traits, properties, and performance: how woody plants combine hydraulic and mechanical functions in a cell, tissue, or whole plant. New Phytol. 204, 747–764. https://doi.org/10.1111/nph.13035.
Lautner, S., Fromm, J., 2010. Calcium-dependent physiological processes in trees. Plant Biol. 12, 268–274. https://doi.org/10.1111/j.1438-8677.2009.00281.x.
Liebmann, B., Marengo, J.A., 2001. Interannual variability of the rainy season and rainfall in the brazilian Amazon Basin. J. Clim. 14, 4308–4318. https://doi.org/10.1175/1520-0442(2001)014<4308:IVOTRS>2.0.CO;2.
Lobão, M.S., 2011. Dendrocronologia , fenologia , atividade cambial e qualidade do lenho de árvores de Cedrela odorata L., Cedrela fissilis Vell. e Schizolobium parahyba var. amazonicum Hub. ex Ducke, no estado do Acre. Brasil. 215.
Lopez, L., Stahle, D., Villalba, R., Torbenson, M., Feng, S., Cook, E., 2017. Tree ring reconstructed rainfall over the southern Amazon Basin. Geophys. Res. Lett. 44, 7410–7418. https://doi.org/10.1002/2017GL073363.
Lovejoy, T.E., Nobre, C., 2018. Amazon tipping point. Sci. Adv., eaat2340 https://doi.org/10.1126/sciadv.aat2340.
Malhi, Y., Roberts, T., Betts, R.A., 2008. Climate change and the fate of the Amazon - preface. Philos. Trans. R. Soc. B-Biological Sci. 363, 1727.
Malhi, Y., Wood, D., Baker, T.R., Wright, J., Phillips, O.L., Cochrane, T., Meir, P., Chave, J., Almeida, S., Arroyo, L., Higuchi, N., Killeen, T.J., Laurance, S.G., Laurance, W.F., Lewis, S.L., Monteagudo, A., Neill, D.A., Vargas, P.N., Pitman, N.C.A., Quesada, C.A., Salomão,

R., Silva, J.N.M., Lezama, A.T., Terborgh, J., Martínez, R.V., Vinceti, B., 2006. The regional variation of aboveground live biomass in old-growth amazonian forests. Glob. Chang. Biol. 12, 1107–1138. https://doi.org/10.1111/j.1365-2486.2006.01120.x.

Mantua, N.J., Hare, S.R., 2002. The Pacific decadal oscillation. J. Oceanogr. https://doi.org/10.1023/A:1015820616384.

Marengo, J.A., 2004. Interdecadal variability and trends of rainfall across the Amazon basin. Theor. Appl. Climatol. 78, 79–96. https://doi.org/10.1007/s00704-004-0045-8.

Marengo, J.A., Espinoza, J.C., 2016. Extreme seasonal droughts and floods in Amazonia: causes, trends and impacts. Int. J. Climatol. 36, 1033–1050. https://doi.org/10.1002/JOC.4420.

Marengo, J.A., Liebmann, B., Grimm, A.M., Misra, V., Silva Dias, P.L., Cavalcanti, I.F.A., Carvalho, L.M.V., Berbery, E.H., Ambrizzi, T., Vera, C.S., Saulo, A.C., Nogues-Paegle, J., Zipser, E., Seth, A., Alves, L.M., 2012. Recent developments on the South American monsoon system. Int. J. Climatol. https://doi.org/10.1002/joc.2254.

Marengo, J.A., Nobre, C.A., Sampaio, G., Salazar, L.F., Borma, L.S., 2011. Climate change in the Amazon Basin: Tipping points, changes in extremes, and impacts on natural and human systems. In: Bush, M.B., Flenley, J.R., Gosling, W.D. (Eds.), Tropical Rainforest Responses to Climatic Change. Springer-Verlag, Berlin Heidelberg, pp. 259–283 https://doi.org/10.1007/978-3-642-05383-2_9.

Marengo, J.A., Nobre, C.A., Tomasella, J., Cardoso, M.F., Oyama, M.D., 2008. Hydro-climatic and ecological behaviour of the drought of Amazonia in 2005. Philos. Trans. R. Soc., B, 1773–1778 https://doi.org/10.1098/rstb.2007.0015.

Marengo, J.A., Rogers, J.C., 2001. Polar air outbreaks in the Americas: assessments and impacts during modern and past climates. In: Markgraf, V. (Ed.), Interhemispheric Climate Linkages. Academic Press, San Diego, pp. 31–51.

Marengo, J.A., Souza, C., 2018. Climate Change: Impacts and Scenarios for the Amazon. Sao Paulo.

Marengo, J.A., Souza, C.M., Thonicke, K., Burton, C., Halladay, K., Betts, R.A., Alves, L.M., Soares, W.R., 2018. Changes in climate and land use over the Amazon region: current and future variability and trends. Front. Earth Sci. 6. https://doi.org/10.3389/feart.2018.00228.

Marengo, J.A., Williams, E.R., Alves, L.M., Soares, W.R., Rodriguez, D.A., 2016. Extreme seasonal climate variations in the Amazon Basin: droughts and floods. In: Nagy, L., Forsberg, B.R., Artaxo, P. (Eds.), Interactions Between Biosphere, Atmosphere and Human Land Use in the Amazon Basin. Springer Berlin, Berlin, Heidelberg, pp. 55–78 https://doi.org/10.1007/978-3-662-49902-3.

Marengo, J., Nobre, C.A., Betts, R.A., Cox, P.M., Sampaio, G., Salazar, L., 2009. Global warming and climate change in amazonia: climate-vegetation feedback and impacts on water resources. In: Keller, Bustamante, Michael, Gash, Michael, John Silva Dias, P. (Eds.), Amazonia and Global Change. American Geophysical Union, pp. 273–292 https://doi.org/10.1029/2008GM000743.

Mendivelso, H.A., Camarero, J.J., Gutiérrez, E., Zuidema, P.A., 2014. Time-dependent effects of climate and drought on tree growth in a neotropical dry forest: short-term tolerance vs. long-term sensitivity. Agric. For. Meteorol. 188, 13–23. https://doi.org/10.1016/j.agrformet.2013.12.010.

Menezes, I.R.N., Aragão, J.R.V., Pagotto, M.A., Lisi, C.S., 2022. Teleconnections and edaphoclimatic effects on tree growth of Cedrela odorata L. In a seasonally dry tropical forest in Brazil. Dendrochronologia 72, 125923. https://doi.org/10.1016/J.DENDRO.2022.125923.

MMA - Ministério Do Meio Ambiente, 2005. Plano de manejo da Floresta Nacional do Jamari. Vol. I.. IBAMA, Brasilia.

Morales, M.S., Cook, E.R., Barichivich, J., Christie, D.A., Villalba, R., LeQuesne, C., Srur, A.M., Eugenia Ferrero, M., González-Reyes, Á., Couvreux, F., Matskovsky, V., Aravena, J.C., Lara, A., Mundo, I.A., Rojas, F., Prieto, M.R., Smerdon, J.E., Bianchi, L.O., Masiokas, M.H., Urrutia-Jalabert, R., Rodriguez-Catón, M., Muñoz, A.A., Rojas-Badilla, M., Alvarez, C., Lopez, L., Luckman, B.H., Lister, D., Harris, I., Jones, P.D., Park Williams, A., Velazquez, G., Aliste, D., Aguilera-Betti, I., Marcotti, E., Flores, F., Muñoz, T., Cuq, E., Boninsegna, J.A., 2020. Six hundred years of south american tree rings reveal an increase in severe hydroclimatic events since mid-20th century. Proc. Natl. Acad. Sci. U. S. A. 117, 16816–16823. https://doi.org/10.1073/pnas.2002411117.

Moreira, L.S., Moreira-Turcq, P., Cordeiro, R.C., Turcq, B., Aniceto, K.C., Moreira-Ramírez, M., Cruz, A.P.S., Caquineau, S., Silva, V.C., 2020. Climate and hydrologic controls on late holocene sediment supply to an Amazon floodplain lake. J. Paleolimnol. 64, 389–403. https://doi.org/10.1007/s10933-020-00144-y.

Nobre, C.A., Sampaio, G., Borma, L.S., Castilla-Rubio, J.C., Silva, J.S., Cardoso, M., 2016. Land-use and climate change risks in the amazon and the need of a novel sustainable development paradigm. Proc. Natl. Acad. Sci. U. S. A. 113, 10759–10768. https://doi.org/10.1073/pnas.1605516113.

Nobre, P., Shukla, J., 1996. Variations of sea surface temperature, wind stress, and rainfall over the tropical Atlantic and South America. J. Clim. 9, 2464–2479. https://doi.org/10.1175/1520-0442(1996)009<2464:VOSSTW>2.0.CO;2.

Novello, V.F., Cruz, F.W., Moquet, J.S., Vuille, M., de Paula, M.S., Nunes, D., Edwards, R.L., Cheng, H., Karmann, I., Utida, G., Stríkis, N.M., Campos, J.L.P.S., 2018. Two millennia of South Atlantic convergence zone variability reconstructed from isotopic proxies. Geophys. Res. Lett. 45, 5045–5051. https://doi.org/10.1029/2017GL076838.

Novello, V.F., Cruz, F.W., Vuille, M., Stríkis, N.M., Edwards, R.L., Cheng, H., Emerick, S., De Paula, M.S., Li, X., Barreto, E.D.S., Karmann, I., Santos, R.V., 2017. A high-resolution history of the south american monsoon from last glacial maximum to the holocene. Sci. Rep. 7, 1–8. https://doi.org/10.1038/srep44267.

Oliveira, L.J.C., Costa, M.H., Soares-Filho, B.S., Coe, M.T., 2013. Large-scale expansion of agriculture in Amazonia may be a no-win scenario. Environ. Res. Lett. 8. https://doi.org/10.1088/1748-9326/8/2/024021.

OriginLab Corporation, 2018. Origin Version 2018.

Ortega Rodriguez, D.R., Hevia, A., Sánchez-Salguero, R., Santini, L., de Carvalho, H.W.P., Roig, F.A., Tomazello-Filho, M., 2022. Exploring wood anatomy, density and chemistry profiles to understand the tree-ring formation in Amazonian tree species. Dendrochronologia 71, 125915. https://doi.org/10.1016/J.DENDRO.2021.125915.

Ostrom, C.W., 1990. Time series analysis (regression techniques). J. R. Stat. Soc. Ser. D 40, 453–455. https://doi.org/10.2307/2348738.

Pereira, G.de A., Barbosa, A.C.M.C., Torbenson, M.C.A., Stahle, D.W., Granato-Souza, D., Santos, R.M.Dos, Barbosa, J.P.D., 2018. The climate response of Cedrela Fissilis annual ring width in the Rio São Francisco Basin, Brazil. Tree-Ring Res. 74, 162–171. https://doi.org/10.3959/1536-1098-74.2.162.

Poulter, B., Hattermann, F., Hawkins, E., Zaehle, S., Sitch, S., Restrepo-Coupe, N., Heyder, U., Cramer, W., 2010. Robust dynamics of Amazon dieback to climate change with perturbed ecosystem model parameters. Glob. Chang. Biol. 16, 2476–2495. https://doi.org/10.1111/j.1365-2486.2009.02157.x.

Poussart, P.M., Myneni, S.C.B., Lanzirotti, A., 2006. Tropical dendrochemistry: a novel approach to estimate age and growth from ringless trees. Geophys. Res. Lett. 33, 1–5. https://doi.org/10.1029/2006GL026929.

Pucha-Cofrep, D., Peters, T., Bräuning, A., 2015. Wet season precipitation during the past century reconstructed from tree-rings of a tropical dry forest in southern Ecuador. Glob. Planet. Chang. 133, 65–78. https://doi.org/10.1016/j.gloplacha.2015.08.003.

Quintilhan, M.T., Santini, L., Ortega Rodriguez, D.R., Guillemot, J., Cesilio, G.H.M., Chambi-Legoas, R., Nouvellon, Y., Tomazello-Filho, M., 2021. Growth-ring boundaries of tropical tree species: aiding delimitation by long histological sections and wood density profiles. Dendrochronologia 125878. https://doi.org/10.1016/J.DENDRO.2021.125878.

Team, R.Core, 2021. R: A Language and Environment for Statistical Computing. R Found. Stat. Comput.

R Core Team, 2019. R: A Language and Environment for Statistical Computing. R Found. Stat. Comput.

Reboita, M.S., Santos, I., 2015. Influência de alguns padrões de teleconexão na precipitação no norte nordeste do brasil. Rev. Bras. Climatol. 15. https://doi.org/10.5380/abclima.v15i0.37686.

Ritchie, P.D.L., Parry, I., Clarke, J.J., Huntingford, C., Cox, P.M., 2022. Increases in the temperature seasonal cycle indicate long-term drying trends in Amazonia. Commun. Earth Enviroment https://doi.org/10.1038/s43247-022-00528-0.

Rodriguez-Caton, M., Andreu-Hayles, L., Daux, V., Vuille, M., Varuolo-Clarke, A.M., Oelkers, R., Christie, D.A., D'Arrigo, R., Morales, M.S., Palat Rao, M., Srur, A.M., Vimeux, F., Villalba, R., 2022. Hydroclimate and ENSO variability recorded by oxygen isotopes from tree rings in the south american altiplano. Geophys. Res. Lett. 49. https://doi.org/10.1029/2021GL095883.

Rodriguez-Caton, M., Andreu-Hayles, L., Morales, M.S., Daux, V., Christie, D.A., Coopman, R.E., Alvarez, C., Rao, M.P., Aliste, D., Flores, F., Villalba, R., 2021. Different climate sensitivity for radial growth, but uniform for tree-ring stable isotopes along an aridity gradient in polylepis tarapacana, the world's highest elevation tree species. Tree Physiol. 41, 1353–1371. https://doi.org/10.1093/treephys/tpab021.

Rodríguez-Fonseca, B., Polo, I., García-Serrano, J., Losada, T., Mohino, E., Mechoso, C.R., Kucharski, F., 2009. Are Atlantic Niños enhancing Pacific ENSO events in recent decades? Geophys. Res. Lett. 36. https://doi.org/10.1029/2009GL040048.

Sánchez-Salguero, R., Camarero, J.J., Hevia, A., Sangüesa-Barreda, G., Galván, J.D., Gutiérrez, E., 2019. Testing annual tree-ring chemistry by X-ray fluorescence for dendroclimatic studies in high-elevation forests from the Spanish Pyrenees. Quat. Int. 514, 130–140. https://doi.org/10.1016/j.quaint.2018.09.007.

Santos, G.M., Ortega Rodriguez, D.R., Barreto, N.D., Assis-Pereira, G., Barbosa, A.C., Roig, F.A., Tomazello-Filho, M., 2021. Growth assessment of native tree species from the southwestern Brazilian Amazonia by Post-AD 1950 14 C Analysis: Implications for Tropical Dendroclimatology Studies and Atmospheric 14 C Reconstructions.

Schöngart, J., Wittmann, F., Faria de Resende, A., Assahira, C., de Sousa Lobo, G., Rocha Duarte Neves, J., da Rocha, M., Biem Mori, G., Costa Quaresma, A., Oreste Demarchi, L., Weiss Albuquerque, B., Oliveira Feitosa, Y., da Silva Costa, G., Vieira Feitoza, G., Machado Durgante, F., Lopes, A., Trumbore, S.E., Sanna Freire Silva, T., ter Steege, H., Val, A.L., Junk, W.J., Piedade, M.T.F., 2021. The shadow of the Balbina dam: A synthesis of over 35 years of downstream impacts on floodplain forests in Central Amazonia. Aquat. Conserv. Mar. Freshw. Ecosyst. 31, 1117–1135. https://doi.org/10.1002/aqc.3526.

Schongart, J., Wolfgang, J.J., Piedade, M., Ayres, J., Huttermann, A., Worbes, M., 2004. Teleconnection between tree growth in the Amazonian floodplains and the El Niño-southern oscillation effect. Glob. Chang. Biol. 10, 683–692. https://doi.org/10.1111/j.1529-8817.2003.00754.x.

Schulman, E., 1956. Dendroclimatic Changes in Semi-arid America. University. ed. University of Arizona Press, Tucson, Arizona.

Schweingruber, F.H., Fritts, H.C., Braker, O.U., Drew, L.G., Schar, E., 1978. The X-ray technique as applied to dendroclimatology. Tree-Ring Bull. 38, 61–91.

Segura, H., Espinoza, J.C., Junquas, C., Lebel, T., Vuille, M., Garreaud, R., 2020. Recent changes in the precipitation-driving processes over the southern tropical Andes/western Amazon. Clim. Dyn. 54, 2613–2631. https://doi.org/10.1007/s00382-020-05132-6.

Smith, K.T., Shortle, W.C., 1996. Tree biology and dendrochemistry. In: Dean, J.S., Meko, D.M., Swetnam, T.W. (Eds.), Tree Rings, Environment and Humanity. Radiocarbon, pp. 629–635.

Stahle, D.W., Torbenson, M.C.A., Howard, I.M., Granato-Souza, D., Barbosa, A.C., Feng, S., Schöngart, J., Lopez, L., Villalba, R., Villanueva, J., Fernandes, K., 2020. Pan american interactions of Amazon precipitation, streamflow, and tree growth extremes. Environ. Res. Lett. 15. https://doi.org/10.1088/1748-9326/ababc6.

Stokes, M.A., Smiley, T.L., 1996. An Introduction to tree-ring Dating.

Tomazello-Filho, M., Brazolin, S., Chagas, M.P., Oliveira, J.T.S., Ballarin, A.W., Benjamin, C.A., 2008. Application of X-ray technique in nondestructive evaluation of eucalypt wood. Maderas. Cienc. Tecnol. 10, 139–149. https://doi.org/10.4067/S0718-221X2008000200006.

Torralba, V., Rodríguez-Fonseca, B., Mohino, E., Losada, T., 2015. The non-stationary influence of the Atlantic and Pacific niños on north eastern South American rainfall. Front. Earth Sci. 3, 1–10. https://doi.org/10.3389/feart.2015.00055.

Torrence, C., Compo, G.P., 1998. A practical guide to wavelet analysis. Bull. Am. Meteorol. Soc. 79, 61–78. https://doi.org/10.1175/1520-0477(1998)079<0061:APGTWA>2.0.CO;2.

Torrence, C., Webster, P.J., 1999. Interdecadal changes in the ENSO-monsoon system. J. Clim. 12, 2679–2690. https://doi.org/10.1175/1520-0442(1999)012<2679:icitem>2.0.co;2.
Vicente-Serrano, S.M., Beguería, S., López-Moreno, J.I., 2010. A multiscalar drought index sensitive to global warming: the standardized precipitation evapotranspiration index. J. Clim. 23, 1696–1718. https://doi.org/10.1175/2009JCLI2909.1.
Volland, F., Pucha, D., Bräuning, A., 2016. Hydro-climatic variability in southern Ecuador reflected by tree-ring oxygen isotopes. Erdkunde 70, 69–82. https://doi.org/10.3112/erdkunde.2016.01.05.
Vuille, M., Burns, S.J., Taylor, B.L., Cruz, F.W., Bird, B.W., Abbott, M.B., Kanner, L.C., Cheng, H., Novello, V.F., 2012. A review of the south american monsoon history as recorded in stable isotopic proxies over the past two millennia. Clim. Past https://doi.org/10.5194/cp-8-1309-2012.
Vuille, M., Werner, M., 2005. Stable isotopes in precipitation recording south american summer monsoon and ENSO variability: observations and model results. Clim. Dyn. 25, 401–413. https://doi.org/10.1007/s00382-005-0049-9.
Wang, C., Enfield, D.B., 2003. A further study of the tropical Western Hemisphere warm pool. J. Clim. 16, 1476–1493. https://doi.org/10.1175/1520-0442-16.10.1476.
Wang, C., Enfield, D.B., 2001. The tropical western hemisphere warm pool. Geophys. Res. Lett. 28, 1635–1638. https://doi.org/10.1029/2000GL011763.
Wang, X., Edwards, R.L., Auler, A.S., Cheng, H., Kong, X., Wang, Y., Cruz, F.W., Dorale, J.A., Chiang, H.W., 2017. Hydroclimate changes across the Amazon lowlands over the past 45,000 years. Nature 541, 204–207. https://doi.org/10.1038/nature20787.
Weisberg, S., 1987. Applied linear regression. Biometrics 43, 258. https://doi.org/10.2307/2531984.
Wieloch, T., Helle, G., Heinrich, I., Voigt, M., Schyma, P., 2011. A novel device for batch-wise isolation of α-cellulose from small-amount wholewood samples. Dendrochronologia 29, 115–117. https://doi.org/10.1016/j.dendro.2010.08.008.
Wigley, T.M.L., Briffa, K.R., Jones, P.D, 1984. On the average value of correlated time series, with applications in dendroclimatology and hydrometeorology. J. Clim. Appl. Meteorol. https://doi.org/10.1175/1520-0450(1984)023<0201:OTAVOC>2.0.CO;2.
Worbes, M., Klosa, D., Lewark, S., 1995. Rohdichtestruktur von jahresringen tropischer Hölzer aus zentralamazonischen Überschwemmungswäldern. Holz als Roh- und Werkst. 53, 63–67. https://doi.org/10.1007/BF02716390.
Yuan, Z.Y., Jiao, F., Shi, X.R., Sardans, J., Maestre, F.T., Delgado-Baquerizo, M., Reich, P.B., Peñuelas, J., 2017. Experimental and observational studies find contrasting responses of soil nutrients to climate change. elife 6, 1–19. https://doi.org/10.7554/eLife.23255.
Zang, C., Biondi, F., 2015. Treeclim: an R package for the numerical calibration of proxy-climate relationships. Ecography (Cop.) 38, 431–436. https://doi.org/10.1111/ecog.01335.
Zhou, J., Lau, K.M., 2001. Principal modes of interannual and decadal variability of summer rainfall over South America. Int. J. Climatol. 21, 1623–1644. https://doi.org/10.1002/joc.700.